Climate Dynamics (1998) 14:571–591

B. Dong · P. J. Valdes

Simulations of the Last Glacial Maximum climates using a general circulation model: prescribed versus computed sea surface temperatures

Received: 10 January 1997/Accepted: 11 December 1997

Abstract The climate during the Last Glacial Maximum (LGM) has been simulated using the UK Universities Global Atmospheric Modelling Programme (UGAMP) general circulation model (GCM) with both prescribed sea surface temperatures (SSTs) based on the CLIMAP reconstruction and computed SSTs with a simple thermodynamic slab ocean. Consistent with the Paleoclimate Modelling Intercomparison Project (PMIP), the other boundary conditions include the large changes in ice-sheet topography and geography, a lower sea level, a lower concentration of CO_2 in the atmosphere, and a slightly different insolation pattern at the top of the atmosphere. The results are analysed in terms of changes in atmospheric circulation. Emphasis is given to the changes in surface temperatures, planetary waves, storm tracks and the associated changes in distribution of precipitation. The model responds in a similar manner to the changes in boundary conditions to previous studies in global mean statistics, but differs in its treatment of regional climates. Results also suggest that both the land ice sheets and sea ice introduce significant changes in planetary waves and transient eddy activity, which in turn affect regional climates. The computed SST simulations predict less sea ice and cooler tropical temperatures than those based on CLIMAP SSTs. It is unclear as to whether this is a model and/or a data problem, but the resulting changes in land temperatures and precipitation can be large. Snow mass budget analysis suggests that there is net ice loss along the southern edges of the Laurentide and Fennoscandian ice sheets and net ice gain over other parts of the two ice sheets. The net accumulation is mainly due to the decrease in ablation in the cold climate rather than to the changes in snowfall. The characteristics of the Greenland ice-sheet mass balance in the LGM simulations is also quite different from those in the present-day (PD) simulations. The ablation in the LGM simulations is negligible while it is a very important process in the ice mass budget in the PD simulations.

B. Dong (✉) · P. J. Valdes
Department of Meteorology, University of Reading, Reading, RG6 6BB, UK
E-mail: swsdong@met.reading.ac.uk

1 Introduction

Atmospheric general circulation models (AGCMs) are typically used in paleoclimate studies. Such studies address the mechanisms of climate change, such as that induced by changes in ice-sheet size, ice-sheet elevation, sea surface temperatures (SSTs) and atmospheric composition. Comparison with paleodata tests the reliability of the models under boundary conditions significantly different from the present-day.

The Last Glacial Maximum (LGM) represents an example of extreme cold climate. It is also a period of rich well-dated proxy data both over ocean and land. Studying this period is important to understand how the ice age boundary conditions can influence climate change, in particular to investigate their impact on midlatitude transient and planetary scale circulation, which in turn has a large effect on the distribution of precipitation in mid-high latitudes. There are two approaches to simulate the LGM climate. One is to use the CLIMAP (CLIMAP 1981) reconstructed SSTs as boundary conditions over ocean. This approach was employed by Hansen et al. (1984), Kutzbach and Guetter (1986), Rind (1987), Lautenschlager and Herterich (1990), Joussaume (1993), Ramstein and Joussaume (1995) and Hall et al. (1996b). The other is to predict SST in the most straightforward way by coupling an AGCM to a simple slab ocean model. This approach was employed by Manabe and Broccoli (1985a,b), Broccoli and Manabe (1987), Felzer et al. (1996) and

Webb et al. (1997). However, these mentioned works employed either the prescribed SST approach or predicted SST approach, but not both with the same model. An interesting question raised is how the LGM cooling and the atmospheric circulation depends upon the treatment of the SSTs. This study addresses this question using the UGAMP GCM.

The results of two simulations, in the framework of the Paleoclimate Modelling Intercomparison Project (PMIP) (Joussaume and Taylor 1995), of the LGM climates are presented. Both approaches of treating SSTs are employed. One LGM simulation uses prescribed SSTs deduced from the CLIMAP dataset. The other one computes SSTs using a thermodynamic slab ocean model with prescribed ocean heat transport. Emphasis is given to the changes in midlatitude transient eddy activities and in planetary waves and their role in regional climate changes during the LGM.

2 The model and boundary conditions

The UGAMP GCM is based on the forecast model of the European Centre for Medium Range Weather Forecasts (ECMWF). The version used here is nearly identical to that currently being used in the Atmospheric Model Intercomparison Project (AMIP) which is described in detail by Slingo et al. (1994).

It is a spectral model with a hybrid sigma/pressure coordinate in the vertical, using a triangular truncation in the horizontal. The physical parametrizations in the model are described in Slingo et al. (1994) and they are evaluated on a longitude/latitude grid of 128 by 64 points, where the mesh size is approximately 2.8° for the model truncated at total wave number 42, henceforth referred to as T42. The model has 19 levels in the vertical, 5 of which are within the lowest 150 hPa of the atmosphere (i.e. in the boundary layer).

The land surface temperature and moisture content are calculated using a three layer diffusive model. A no-flux boundary condition at the bottom of the soil model (approximately 3.4 m deep) is used. This is essential for paleoclimate simulation because it allows the land surface temperature and soil moisture to respond fully to the forcing rather than being tied to some current climatologies on long time scales.

The SSTs in the model can be specified or can be predicted directly. In specified mode, the sea-ice edge is prescribed as the $-2\,^{\circ}$C contour in the sea surface temperature. On sea ice itself, the surface temperature is calculated using a simple sea-ice model. This is a purely thermodynamic model in which heat is stored by and diffused vertically across a slab of ice which is 2 m thick. In the prediction mode, the ocean is represented by a 50 m well-mixed layer, with prescribed, seasonally varying ocean heat flux transport. The ocean heat transport is diagnosed separately over ocean and sea ice from the present-day simulation with the climatological SSTs. Sea ice forms when ocean temperature falls below $-2\,^{\circ}$C. More details of the model were given in Dong and Valdes (1995).

An interactive surface hydrology is employed. Snow cover is computed as the balance of snow fall, snow melting and sublimation. Surface albedo and roughness length are prescribed. When there is snow cover the surface albedo is weighted by snow albedo, which is snow depth dependent. The deep snow (at infinite depth) albedo is 0.8. Over water the surface albedo is 0.07, and over sea ice it is 0.55.

The model is modified for the LGM simulation by changing ice-sheet topography and orography, CO_2 concentration, and the orbital parameters, all the changes are consistent with the PMIP experiments. For the LGM simulation with prescribed SSTs, these are taken from the CLIMAP reconstruction. The CLIMAP data is for February and August. To obtain a seasonally varying SST and sea-ice edge, a similar method to Rind and Peteet (1985) is used, i.e., a simple sinusoidal variation, with extremes in February and August. The land ice-sheet extent and elevation are based on Peltier's (1994) reconstructions, which is given in Fig. 1 for our model at T42 resolution. CO_2 concentration is set to 200 ppm, and the orbital parameters are set to those appropriate for 21 ky ago.

Four integrations have been performed: two simulations for PD (present-day) and two for LGM, with both prescribed and computed SSTs. The two simulations with prescribed SSTs have been run for 11 years and the analysis is based on the last 10 year average. The two simulations with computed SSTs have been run for 21 y. There is no apparent trend and year to year variations in the global mean ocean surface temperatures equilibrated to within 0.2 °C for both PD and LGM simulations with computed SSTs after 1 y and 3 y spinup respectively. Therefore, the analysis for the simulations with computed SSTs is based on the last 20 y average for PD and the last 18 y average for LGM. The small year to year variability in global mean ocean surface temperatures is indicated by small interannual standard deviations given in Table 1. Because the changes of the climate in the LGM simulations relative to the present day simulations are far above the level of the model climate natural variability, we will not discuss the statistical significance level for each quantity presented.

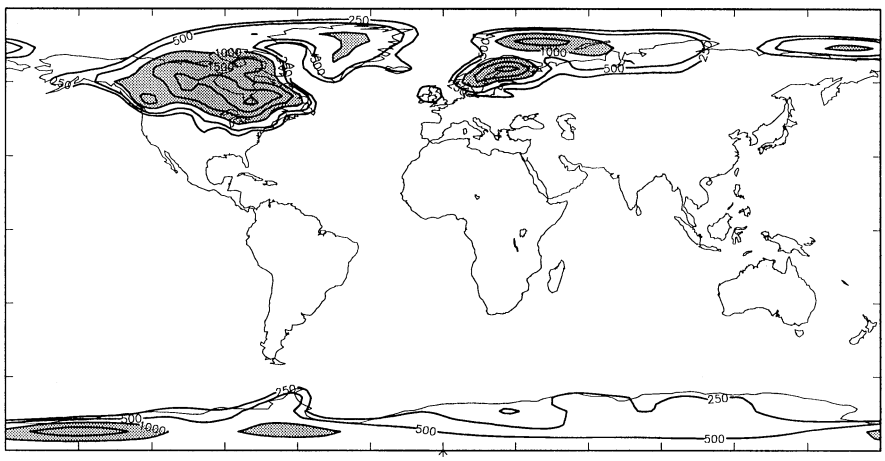

Fig. 1 Changes in ice sheet height and extent of the updated ice sheets (Peltier 1994) at the Last Glacial Maximum (LGM). Contours are at 250, 500 m, and then increasing by 500 m

Table 1 Annually global averaged surface quantities and their standard deviations (in bracket)

	Prescribed SSTs			Computed SSTs		
	PD	LGM	LGM-PD	PD	LGM	LGM-PD
Surface temperature (°C)						
Global	14.4 (0.06)	10.5 (0.04)	− 3.9	14.6 (0.14)	10.3 (0.08)	− 4.3
Land	8.7 (0.22)	1.8 (0.10)	− 6.9	8.9 (0.36)	1.8 (0.18)	− 7.1
Ocean	16.6 (0.02)	15.0 (0.03)	− 1.6	16.9 (0.07)	15.3 (0.07)	− 1.6
2 m air temperature (°C)						
Global	13.5 (0.07)	9.8 (0.08)	− 3.7	13.8 (0.15)	9.6 (0.09)	− 4.2
Land	9.2 (0.21)	2.5 (0.10)	− 6.7	9.4 (0.35)	1.2 (0.18)	− 8.2
Ocean	15.2 (0.02)	13.5 (0.02)	− 1.7	15.5 (0.08)	13.8 (0.07)	− 1.7
Vertically averaged air temperature (°C)						
Global	− 21.4 (0.03)	− 22.9 (0.02)	− 1.5	− 21.2 (0.14)	− 22.9 (0.08)	− 1.7
Land	− 22.4 (0.06)	− 24.5 (0.04)	− 2.1	− 22.3 (0.16)	− 24.7 (0.09)	− 2.4
Ocean	− 21.0 (0.03)	− 22.0 (0.03)	− 1.0	− 20.8 (0.14)	− 22.0 (0.08)	− 1.2
Total precipitation (mm/day)						
Global	2.76 (0.010)	2.54 (0.008)	− 0.22	2.76 (0.007)	2.58 (0.014)	− 0.18
Land	2.47 (0.020)	1.96 (0.031)	− 0.51	2.45 (0.045)	2.12 (0.044)	− 0.33
Ocean	2.87 (0.013)	2.83 (0.015)	− 0.04	2.88 (0.014)	2.82 (0.021)	− 0.06
Convective precipitation (mm/day)						
Global	2.09 (0.009)	1.86 (0.008)	− 0.23	2.10 (0.010)	1.90 (0.013)	− 0.20
Land	1.93 (0.019)	1.43 (0.028)	− 0.50	1.90 (0.039)	1.58 (0.040)	− 0.32
Ocean	2.16 (0.012)	2.09 (0.017)	− 0.07	2.18 (0.017)	2.06 (0.024)	− 0.12
Evaporation (mm/day)						
Global	2.77 (0.01)	2.56 (0.009)	− 0.21	2.78 (0.006)	2.60 (0.014)	− 0.18
Land	1.03 (0.02)	0.81 (0.016)	− 0.22	1.02 (0.020)	0.83 (0.016)	− 0.19
Ocean	3.45 (0.01)	3.45 (0.009)	0.00	3.47 (0.007)	3.50 (0.017)	0.03
Snow fall (mm/day)						
Global	0.23 (0.003)	0.30 (0.003)	0.07	0.22 (0.004)	0.30 (0.005)	0.08
Land	0.31 (0.007)	0.37 (0.007)	0.06	0.32 (0.010)	0.37 (0.007)	0.05
Ocean	0.20 (0.004)	0.26 (0.002)	0.06	0.18 (0.005)	0.26 (0.009)	0.08
Soil moisture (mm)						
Land	6.83 (0.13)	6.95 (0.14)	0.12	6.78 (0.18)	7.32 (0.06)	0.54
Sea-ice fraction (%)						
Global	5.06	9.21	4.15	4.26	5.47	1.21
Cloud cover (%)						
Global	56.8 (0.10)	54.4 (0.15)	− 2.4	56.8 (0.13)	56.0 (0.18)	− 0.8
Land	49.3 (0.19)	48.7 (0.37)	− 0.6	49.3 (0.39)	50.8 (0.42)	1.5
Ocean	59.7 (0.17)	57.3 (0.12)	− 2.4	59.7 (0.16)	58.7 (0.17)	− 1.0
Precipitable water ($kg\,m^{-2}$)						
Global	23.9 (0.06)	20.6 (0.04)	− 3.3	24.0 (0.22)	20.6 (0.12)	− 3.4
Land	17.6 (0.09)	13.3 (0.10)	− 4.3	17.7 (0.21)	13.4 (0.14)	− 4.3
Ocean	26.3 (0.06)	24.2 (0.05)	− 2.1	26.5 (0.28)	24.2 (0.14)	− 2.3
CRF_S ($W\,m^{-2}$)						
Global	− 60.1 (0.12)	− 51.7 (0.11)	8.4	− 60.4 (0.22)	− 54.1 (0.26)	6.3
Land	− 32.2 (0.22)	− 24.4 (0.33)	7.8	− 32.1 (0.34)	− 25.6 (0.40)	6.5
Ocean	− 70.9 (0.11)	− 65.5 (0.08)	5.4	− 71.4 (0.26)	− 68.5 (0.34)	2.9
CRF_L ($W\,m^{-2}$)						
Global	32.8 (0.08)	30.5 (0.11)	− 2.3	33.0 (0.15)	30.9 (0.20)	− 2.1
Land	27.9 (0.20)	24.1 (0.32)	− 3.8	28.0 (0.32)	24.3 (0.40)	− 3.7
Ocean	34.6 (0.09)	33.7 (0.11)	− 0.9	34.9 (0.20)	34.3 (0.30)	− 0.6
CRF_T ($W\,m^{-2}$)						
Global	− 27.3 (0.10)	− 21.2 (0.08)	6.1	− 27.4 (0.24)	− 23.2 (0.24)	4.2
Land	− 4.3 (0.21)	− 0.3 (0.15)	4.0	− 4.1 (0.21)	− 1.3 (0.24)	2.8
Ocean	− 36.3 (0.13)	− 31.8 (0.16)	4.5	− 36.5 (0.30)	− 34.2 (0.32)	2.3
Greenhouse effect ($W\,m^{-2}$)						
Global	175.9 (0.14)	167.7 (0.10)	− 8.2	176.3 (0.37)	167.5 (0.24)	− 8.8
Land	157.2 (0.23)	144.3 (0.20)	− 12.9	157.4 (0.42)	143.5 (0.39)	− 13.9
Ocean	183.1 (0.12)	179.5 (0.10)	− 3.6	183.7 (0.38)	179.7 (0.22)	− 4.0

3 Global mean changes

The sensitivity of the climate simulation to perturbations in boundary conditions is dependent on the simulation of the unperturbed climate. The validation of the present day climate simulation using the UGAMP GCM was briefly discussed in Dong and Valdes (1995). The main features of the present-day climate were reproduced by the model with both prescribed and computed SSTs. The simulated global annual mean surface temperatures of 14.4 °C and 14.6 °C are very close to the observation of 14.5 °C based on Legates and Willmott (1990) climatology. The patterns of monsoon circulation are reasonable (Dong et al. 1996). The simulated global annual mean precipitation over land is 2.47 and 2.45 mm day^{-1} respectively, which is also close to the observed value of 2.24 mm day^{-1}.

Changes in the boundary conditions have a profound effect on the annual mean climate. Given in Table 1 are the annually averaged values of climatic variables simulated by the model. The global, land and ocean averages are given separately.

The decrease in the globally averaged annual mean surface air temperature is 3.7 °C in the LGM simulations with prescribed SSTs and 4.2 °C with computed SSTs. The cooling is larger over land than over ocean. Over land the cooling is larger in JJA (June, July and August), with decreases of 7.0 and 8.4 °C, than in DJF (December, January and February), which are 6.5 and 8.2 °C, for the prescribed and computed SSTs respectively. This reflects the impact of the large difference in surface albedo in the Northern Hemisphere summer due to the presence of ice sheets at the LGM.

The expected decrease in the vigour of the hydrological cycle is found. The larger decrease occurs over land. Due to the cold climate, the snowfall in the LGM simulation increases by about 30% for the global annual average.

The changes reported here are consistent with previous model simulations (e.g., Hansen et al. 1984; Kutzbach and Guetter 1986; Manabe and Broccoli 1985a; Lautenschlager and Herterich 1990). Hall et al. (1996b) reported a 3.8 °C decrease in the global annual mean surface air temperature and 0.2 mm day^{-1} decrease in the global annual mean precipitation using the UGAMP GCM, but with the CLIMAP ice-sheet reconstruction. This indicates that the global averaged climate change due to ice age boundary conditions is not very sensitive to the ice sheet reconstruction. Ramstein and Joussaume (1995) found similar results using the LMD GCM.

There is less sea-ice in the PD simulation with computed SSTs. This has a local effect, mainly around the Antarctic where SSTs over water are 0.3 °C warmer, but otherwise, the simulated present-day SSTs are very close to the climatological SSTs. Note that this is largely a consequence of our choice of ocean heat flux. For the LGM simulation with computed SSTs, the Southern Hemisphere sea-ice fraction is much lower than that suggested by the CLIMAP reconstruction while it is higher in the Northern Hemisphere. The CLIMAP reconstruction suggests that sea-ice fraction increases by 15.7% in the Northern Hemisphere and by 128.7% in the Southern Hemisphere. The simulation suggests that sea-ice fraction increases by 47.9% in the Northern Hemisphere and only 8.6% in the Southern Hemisphere. This implies that, either the model treatment of sea-ice is in error, or the CLIMAP Southern Hemisphere sea-ice cover may be seriously overestimated, as Burckle et al. (1982) argued.

Cloud feedbacks are important in the response of climate models to perturbed boundary conditions. Generally, shortwave cloud radiative forcing (CRF_S) is overestimated by about 24% in the PD simulations compared to observational studies (Harrison et al. 1990), while longwave cloud radiative forcing (CRF_L) is very close to the observations, leading to total cloud radiative forcing (CRF_T) being overestimated by the model by about 10.0 W m^{-2}. The large inconsistency in CRF_S between the simulations and observations implies that the cloud in the model is too reflective. This will result in a high sensitivity in CRF_S to changes in cloud cover in the LGM simulations.

Global mean total cloud radiative forcing is reduced in the two LGM simulations relative to the PD simulations. This is true for both the DJF and JJA seasons. This positive difference implies a weakening of the mean negative forcing induced by clouds. Quantitatively, the decrease of shortwave cloud radiative forcing (warming effect) in the LGM simulation with prescribed SSTs is larger than that in the simulation with computed SSTs. The main impact of longwave cloud radiative forcing is a reduction of their greenhouse effect in the LGM simulations and this effect is similar in the two simulations. As a result, the difference of the magnitude of total cloud radiative forcing in the two LGM simulations relative to the PD simulations is mainly the result of the differences in the shortwave cloud radiative forcing. A larger decrease in total cloud radiative forcing in the LGM simulation with prescribed SSTs implies a smaller decrease in air temperature.

The percentage changes in cloud radiative forcings in the LGM simulations relative to the PD simulations are significantly larger than percentage changes in total cloud cover. This is related to changes in the vertical distribution in cloud cover. Examination of changes in the vertical distribution of cloud cover (Table 2) suggests that there is a large decrease in both high and convective cloud covers, and an increase in medium cloud cover. These leads to a relatively small decrease in total cloud cover. However, because of the large reflectivity in the solar radiation by high and convective clouds, the decrease in these two types of clouds results in a large decrease in shortwave cloud radiative forcing.

Table 2 Annually global averaged cloud covers and their standard deviations (in bracket)

	Prescribed SSTs			Computed SSTs		
	PD	LGM	LGM-PD	PD	LGM	LGM-PD
High cloud (%)						
Global	30.9 (0.21)	28.7 (0.18)	− 2.2	30.9 (0.16)	30.1 (0.20)	− 0.8
Land	28.2 (0.14)	25.3 (0.36)	− 2.9	28.2 (0.32)	26.6 (0.32)	− 1.6
Ocean	32.0 (0.25)	30.4 (0.18)	− 1.6	32.0 (0.26)	31.9 (0.31)	− 0.1
Medium cloud (%)						
Global	21.7 (0.07)	21.6 (0.08)	− 0.1	21.7 (0.09)	22.3 (0.18)	0.6
Land	24.1 (0.17)	25.6 (0.18)	1.5	24.1 (0.20)	26.4 (0.23)	2.3
Ocean	20.8 (0.06)	19.5 (0.12)	− 1.3	20.7 (0.10)	20.3 (0.18)	− 0.4
Low cloud (%)						
Global	37.2 (0.11)	35.6 (0.09)	− 1.6	37.1 (0.15)	36.2 (0.16)	− 0.9
Land	27.7 (0.30)	28.2 (0.22)	0.5	27.7 (0.34)	29.2 (0.30)	1.5
Ocean	40.9 (0.08)	39.4 (0.05)	− 1.5	40.8 (0.13)	39.7 (0.13)	− 1.1
Convective cloud (%)						
Global	26.8 (0.06)	23.2 (0.08)	− 3.6	27.0 (0.09)	24.2 (0.13)	− 2.8
Land	13.1 (0.12)	9.9 (0.13)	− 3.2	13.0 (0.16)	10.3 (0.17)	− 2.7
Ocean	32.1 (0.05)	30.0 (0.07)	− 2.1	32.4 (0.09)	31.3 (0.16)	− 1.1

Although water vapour is the single most important greenhouse gas, the effect of changes in its tropospheric concentration is considered as a feedback in climate models. The decrease in atmospheric water vapour of 3.3 and 3.4 $kg\,m^{-2}$ in the two LGM simulations are very close to the result (3.0 $kg\,m^{-2}$) of the simulation with the GISS model using the CLIMAP SSTs by Webb et al. (1997). However, in their LGM simulation with computed SSTs, the decrease (8.6 $kg\,m^{-2}$) in atmospheric water vapour is significantly larger than either their simulation with prescribed SSTs or the simulations presented here using the UGAMP GCM. This is probably the main reason why their LGM simulation with predicted SSTs gives a very large global and tropical cooling.

The clear sky greenhouse effect in the PD simulations is in agreement with observational data (179 $W\,m^{-2}$) shown by Raval and Ramanathan (1989). The global cooling due to the ice age boundary conditions produces a positive feedback. The cooler atmosphere contains less water vapour, which in turn, results in further cooling of the atmosphere. Thus the changes in water vapour result in a positive feedback which is slightly stronger in the simulation with computed SSTs. This positive feedback is also stronger over land than over ocean, consistent with the fact that changes in the hydrological cycle in the LGM simulations are larger over land.

In summary, the water vapour changes have a positive feedback and shortwave cloud radiative forcing has a negative feedback in LGM cooling. The smaller negative shortwave cloud radiative feedback and large positive water vapour feedback in the LGM simulation with predicted SSTs than that with prescribed SSTs leads to enhanced cooling.

The seasonal cycle of surface air temperature averaged over the globe, land, and ocean respectively is given in Fig. 2. Due to the large land masses in the Northern Hemisphere, the phase of the seasonal cycle of the global land surface temperature is in phase with that of the Northern Hemisphere land, and this influences the seasonal cycle of the global mean surface air temperature. Slightly larger land air temperature decrease occurs during the Northern Hemisphere summer, reflecting enhanced snow/albedo feedback at this season.

Global ocean air temperature is reduced throughout the year in the two LGM simulations. The global ocean air temperature at the LGM with computed SSTs is 1.5 °C warmer in JJA and 0.5 °C cooler in DJF than those with prescribed SSTs. The JJA difference is mainly the result of the fact that the simulated Antarctic sea ice at the LGM is not as extensive as the CLIMAP data suggested while DJF differences reflect the relatively warm subtropical regions in the CLIMAP reconstruction which are not simulated with the mixed layer ocean model.

Zonal mean sea surface temperature anomalies between LGM and PD simulations are given in Fig. 3. The use of zonal mean emphasizes large-scale thermal patterns. Generally, the patterns of sea surface temperature changes in the two simulations are similar, with the largest cooling entered in the middle and high latitudes of the Northern Hemisphere and second largest cooling in the southern high latitudes in JJA, which are associated with sea ice. However, there are noticeable differences. The larger cooling south of 60 °N in the simulation with computed SSTs is due to more extensive Pacific sea ice. Less extensive sea ice in JJA over southern high latitudes results in less cooling there. The warm anomalies over subtropical regions suggested by the CLIMAP reconstruction is not simulated. It has been suggested that this warmth is a dynamical response of the ocean to changes in

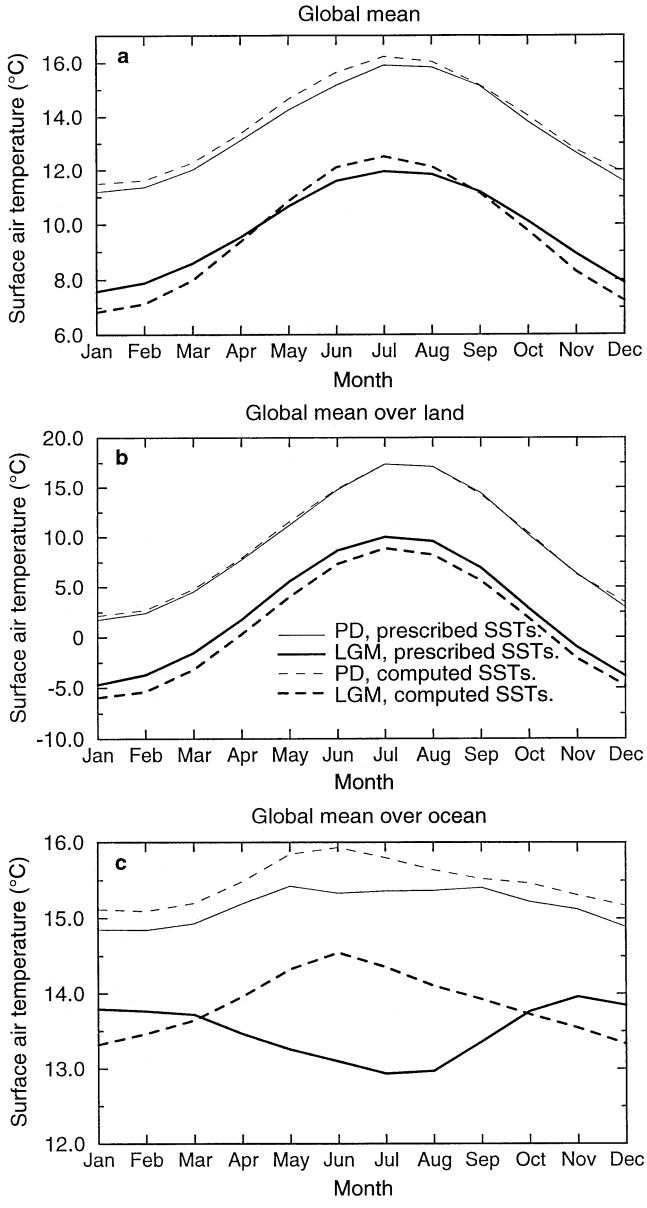

Fig. 2a–c Seasonal cycle of surface air temperature based on monthly mean values for global, land, and ocean means for the PD and LGM simulations

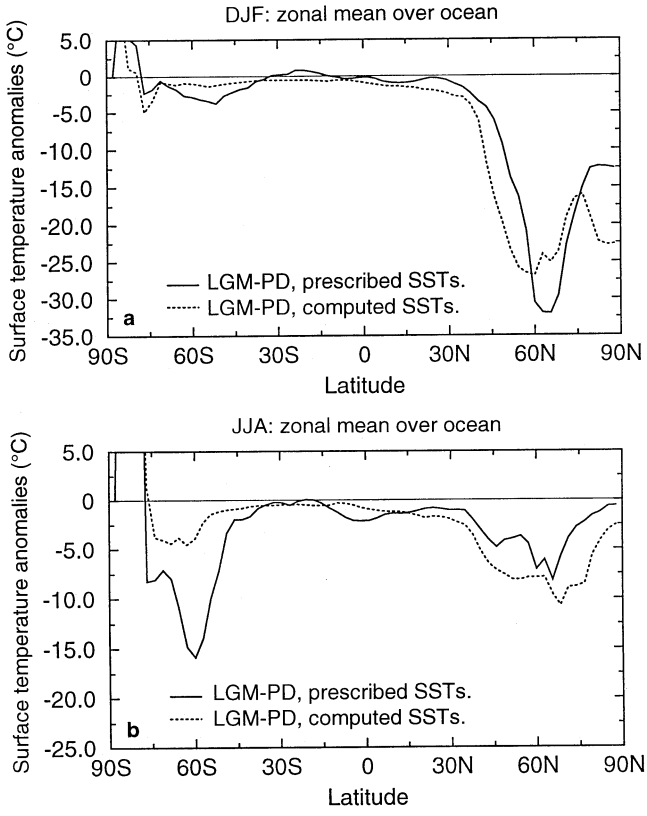

Fig. 3a,b Zonal mean sea surface temperature anomalies between the LGM and PD simulations. **a** DJF and **b** JJA

atmospheric circulation (Moore et al. 1980), in which case the simplified treatment of slab ocean model would preclude its simulation.

4 Regional changes in surface air temperature

The simulated surface air temperature anomalies between the LGM and PD for DJF and JJA are illustrated in Fig. 4. Generally, the cooling is smaller in tropical regions, increases with latitude, reaching maximum values over ice sheets and sea ice. This is true for both LGM simulations with prescribed and computed SSTs. However, the LGM simulation with computed SSTs, over tropical and subtropical oceans, is about 1.0 °C cooler than PD.

In DJF, the largest cooling in the LGM simulations occurs over sea ice. The North Atlantic sector is generally much colder with the sea ice edge extending down to about 45°N while the southward extension of sea ice in the computed SST case is not as extensive as the CLIMAP reconstructions suggest over the northeast Atlantic. However, with computed SSTs there is an extensive cooling over the north Pacific, where the sea-ice edge extends to about 42 °N. The large decrease of temperature at the LGM over the north Atlantic and north Pacific in the simulation with computed SSTs are the results of the low thermal heat capacity of sea ice of 2-m thick in our model. The southward extension of sea-ice in the Northern Hemisphere and large cooling over sea ice result in enhanced equator-pole temperature gradient over the north Atlantic and north Pacific at the LGM. These changes in temperature gradient will result in significant changes in upper level circulation and in storm track activities. These will be discussed in the following sections. The significant discrepancy between the simulations with prescribed and computed SSTs over land occurs over southwest

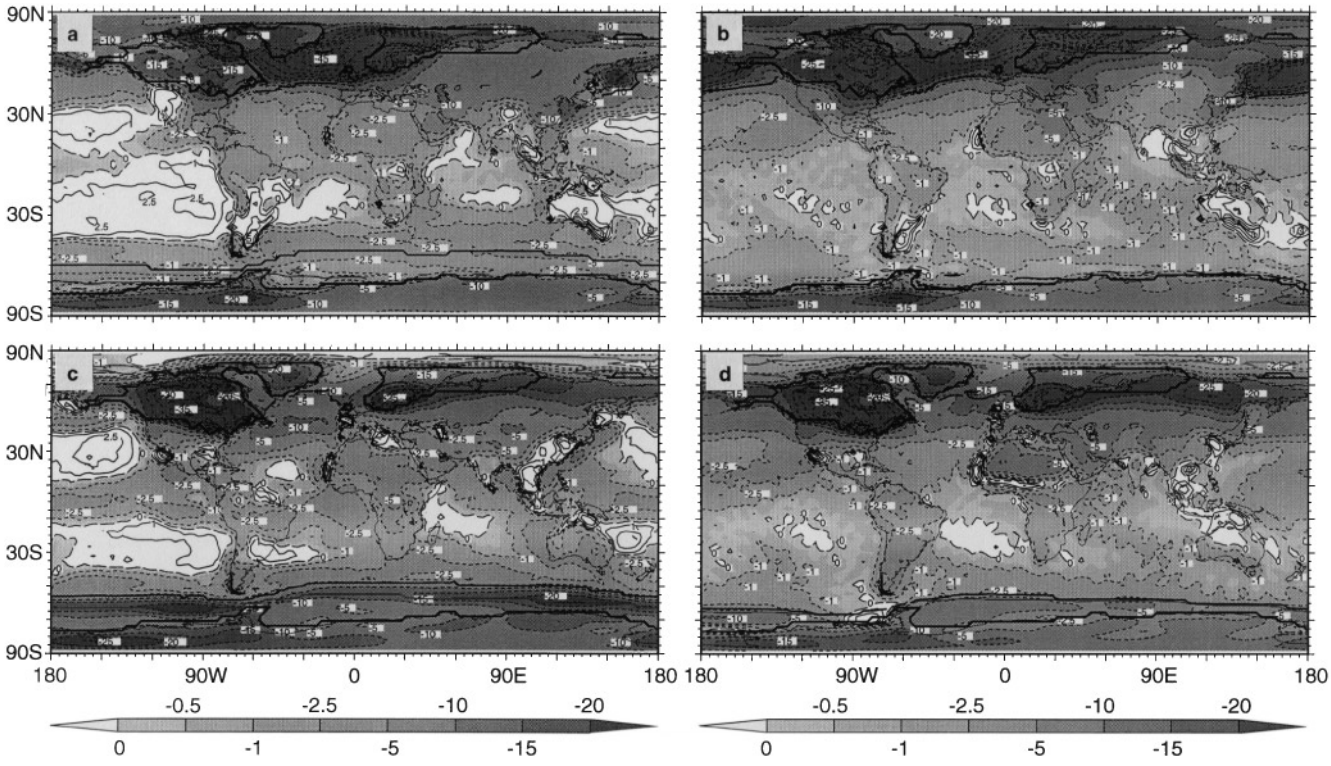

Fig. 4a–d Surface air temperature anomalies (°C) between the LGM and PD simulations. The *thick lines* give the sea-ice edge in PD and LGM simulation, and *dark thick line* the extent of ice sheet at LGM. **a** DJF and **c** JJA with prescribed SSTs. **b** DJF and **d** JJA with computed SSTs

North America and southern South America where the simulation with prescribed SSTs indicates warming and the one with computed SSTs indicates cooling, an effect of circulation changes due to SSTs. This will be discussed in Sect. 5.

In JJA, the largest cooling in the LGM simulations occurs over the two ice sheets, due to both the surface albedo effect and ice elevation effect. The simulations also show a large decrease of surface air temperature over the Siberian regions. This is mainly the result of snow-albedo changes because of the presence of perennial snow cover. As shown in Dong and Valdes (1995), Siberia is a sensitive region of glacial inception in the UGAMP GCM. The simulated sea-ice edge in the LGM over the Southern Hemisphere is 2° to 3° latitude further south than the reconstructions, but this may be explained by the possibility that CLIMAP overestimated the extent of glacial sea ice over the Southern Ocean (Burckle et al. 1982).

In summary, the land air temperature decreases in the LGM simulations with prescribed and computed SSTs are more in agreement in mid- and high latitudes in both DJF and JJA seasons. Over oceans, there is a slight cooling in the tropics and subtropics in the LGM simulation with computed SSTs, which is in contrast to the simulation with the CLIMAP reconstruction that shows a marked warming of the subtropical gyres of the north and south Pacific Ocean. Broccoli and Marciniak (1996), and Hewitt and Mitchell (1996) found a similar disagreement using the GFDL model and the UKMO model.

The simulated cooling in the LGM over mid- and high-latitude lands are reasonably in agreement with the geological evidence as suggested by Velichko et al. (1989). However, over tropical lands, the cooling is underestimated. This is similar to several previous ice age simulations (e.g. Rind and Peteet 1985), and is true for simulations with computed as well as prescribed, CLIMAP SSTs.

5 Response of the atmospheric circulation and planetary waves

5.1 Low level circulation

The distribution of the time-averaged mean sea level (MSL) pressure and 850 hPa winds for PD, LGM and their anomalies are given in Fig. 5 for DJF and Fig. 6 for JJA. (MSL pressure for LGM has been adjusted by subtracting the global averaged MSL pressure difference between the LGM and PD simulations at each grid point). Generally, the overall patterns of MSL

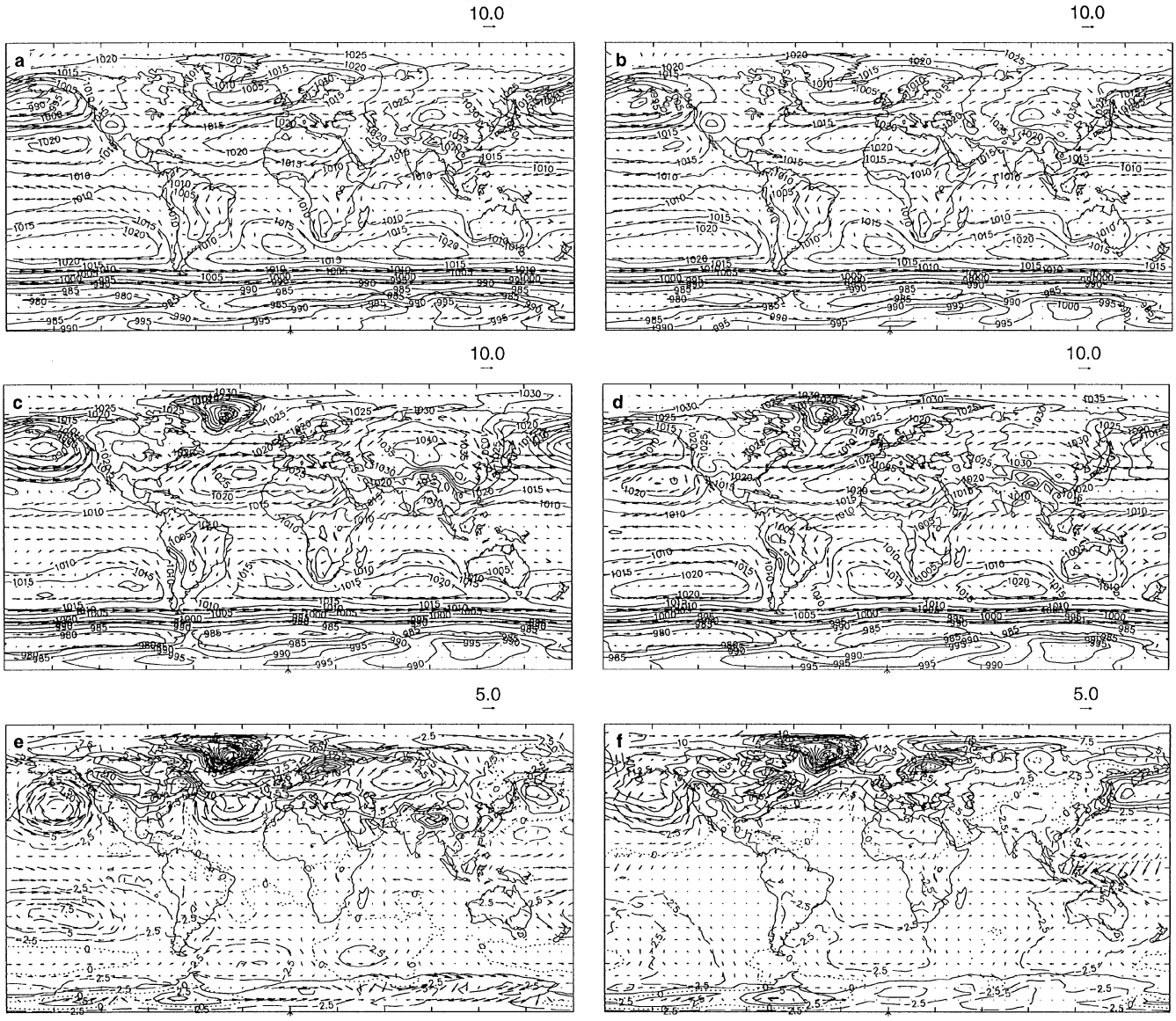

Fig. 5a–f The distribution of mean sea level (MSL) pressure (hPa) and 850 hPa winds (ms^{-1}) in DJF. **a**, **b** PD with prescribed and computed SSTs; **c** and **d** LGM with prescribed and computed SSTs. **e** and **f** the corresponding anomalies between LGM and PD

pressure and wind distribution in tropical and subtropical areas remain unchanged in the LGM simulations. Patterns of MSL pressure and winds over the Southern Hemisphere high latitudes also hardly change. Significant changes occur over northern high latitudes, especially in the winter season.

In DJF, the Azores high is extended more to the west and is enhanced in the LGM simulation with prescribed SSTs, resulting in an enhancement of the westerlies over the north Atlantic along the sea-ice edge. However, in the LGM simulation with computed SSTs, the westward extension of the Azores high is not as strong as the one in the simulation with prescribed SSTs. The low level flow over the north Atlantic appears to be quite sensitive to the position of the sea-ice edge with anomalous anticyclonic circulation with prescribed SSTs and southwesterly with computed SSTs. Glacial anticyclones are located over the Laurentide and Fennoscandian ice sheets and the Iceland low is weakened in the LGM simulations. The Aleutian low is intensified and shifted southward in the LGM simulation with prescribed SSTs, but it is weakened in the LGM simulation with computed SSTs. This difference is once again due to the large difference in sea-ice cover which, over the north Pacific, is more extensive in the LGM simulation with computed SSTs than in the simulation with prescribed SSTs. The intensification of the Aleutian low in the LGM simulation with prescribed SSTs results in an enhancement of southwesterly flow which brings up more tropical air to the west

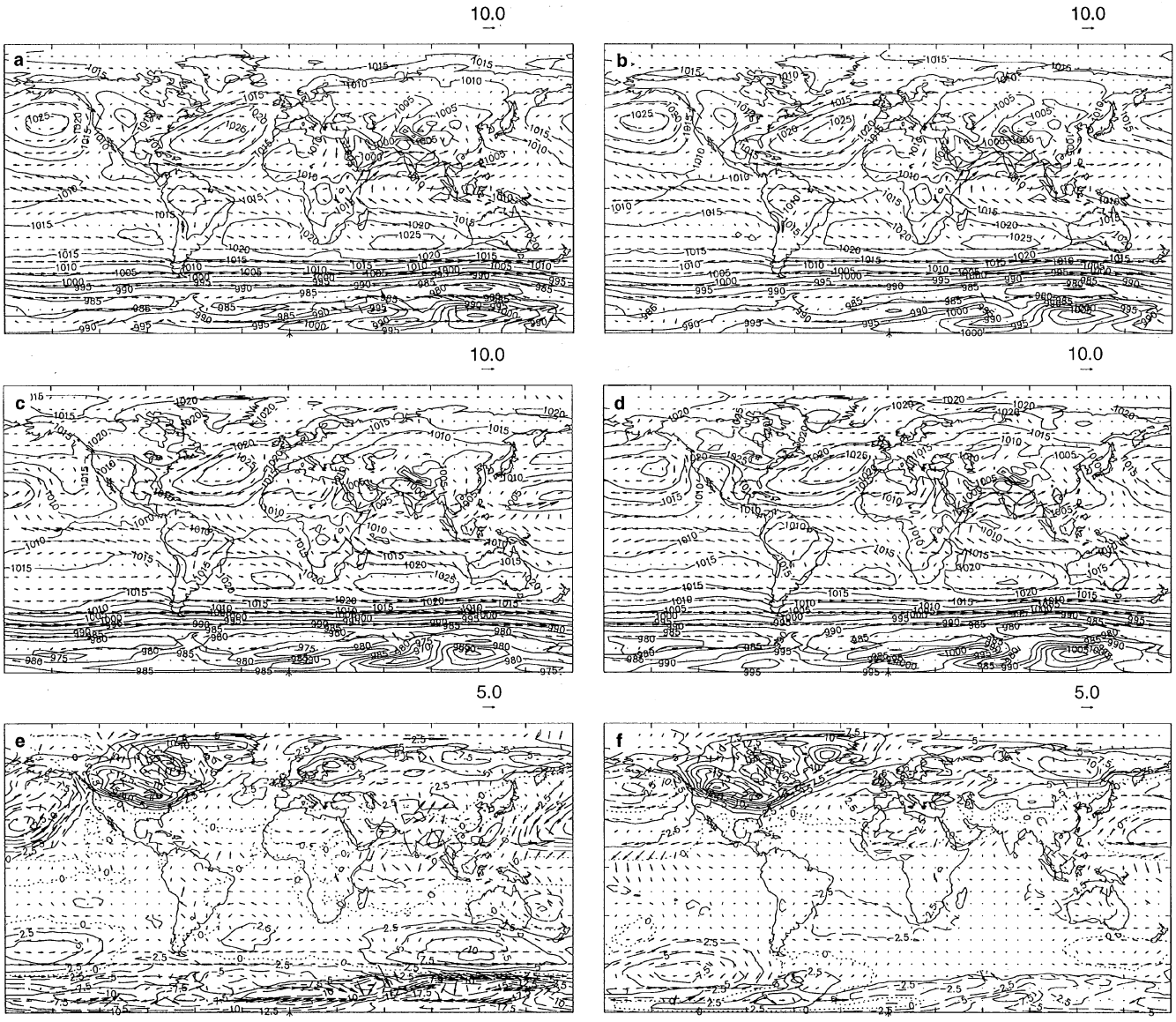

Fig. 6a–f As Fig. 5, but for JJA

coast of North America, where a warming (Fig. 4a) and an increase in precipitation is simulated (Fig. 11a). However, in the LGM simulation with computed SSTs, the southwest flow is weakened and precipitation over the west coast of North America decrease.

In JJA, significant changes occur over the north Pacific-North America sector. MSL pressure over the Laurentide and Fennoscandian ice sheets increase. The high which is normally located south of Alaska in PD is shifted to the south and east and its strength is weakened. This is especially true for the simulation with prescribed SSTs. As a result, the northerlies which blow down the west coast of North America are correspondingly reduced.

The thermal low over southern Asia in the LGM simulation is weakened, which is related to the strong cooling over the Tibetan Plateau. As a result, the southwesterlies over the Arabian Sea and India are weakened, indicating a weaker summer monsoon circulation.

Over South America and the south Atlantic sector, changes in circulation differ in the LGM simulation with prescribed SSTs from the simulation with computed SSTs. In the LGM simulation with prescribed SSTs, the subtropical high over south Atlantic extends westward to the east coast of South America. The lower tropospheric circulation anomalies (Fig. 6e) indicate a divergence of the moisture burden flow over South America in the simulation with prescribed SSTs, whereas they (Fig. 6f) indicate a weak enhanced convergence there in the simulation with computed SSTs. The differences in circulation changes between the simulation

with prescribed SSTs and that with computed SSTs induce differences in precipitation changes, as will be shown in Sect. 7.

5.2 Planetary waves

The planetary waves are of substantial importance to ensure the fidelity of the simulation. The physical processes which contribute to the forcing of the zonal asymmetries include land/ocean contrasts, SST pattern, orographic features, diabatic heating, and synoptic transient eddy activities. At the LGM, large orographic features of the continental ice sheets result in changes of the planetary scale waves. The changes in the transient eddy transport of heat and momentum and in the diabatic heating are also responsible for changes of planetary waves at the LGM.

Shown in Figs. 7 and 8 are the asymmetric stream function and zonal wind at 500 hPa for PD, LGM and the anomalies for DJF and JJA respectively. Both simulations with prescribed and computed SSTs present a credible simulation of the features of planetary waves in DJF and JJA for the PD. The planetary wave patterns are in good agreement with the ECMWF analyses (Hoskins et al. 1989).

In DJF, the LGM simulations show an enhanced wave train across Canada and into the Atlantic. The

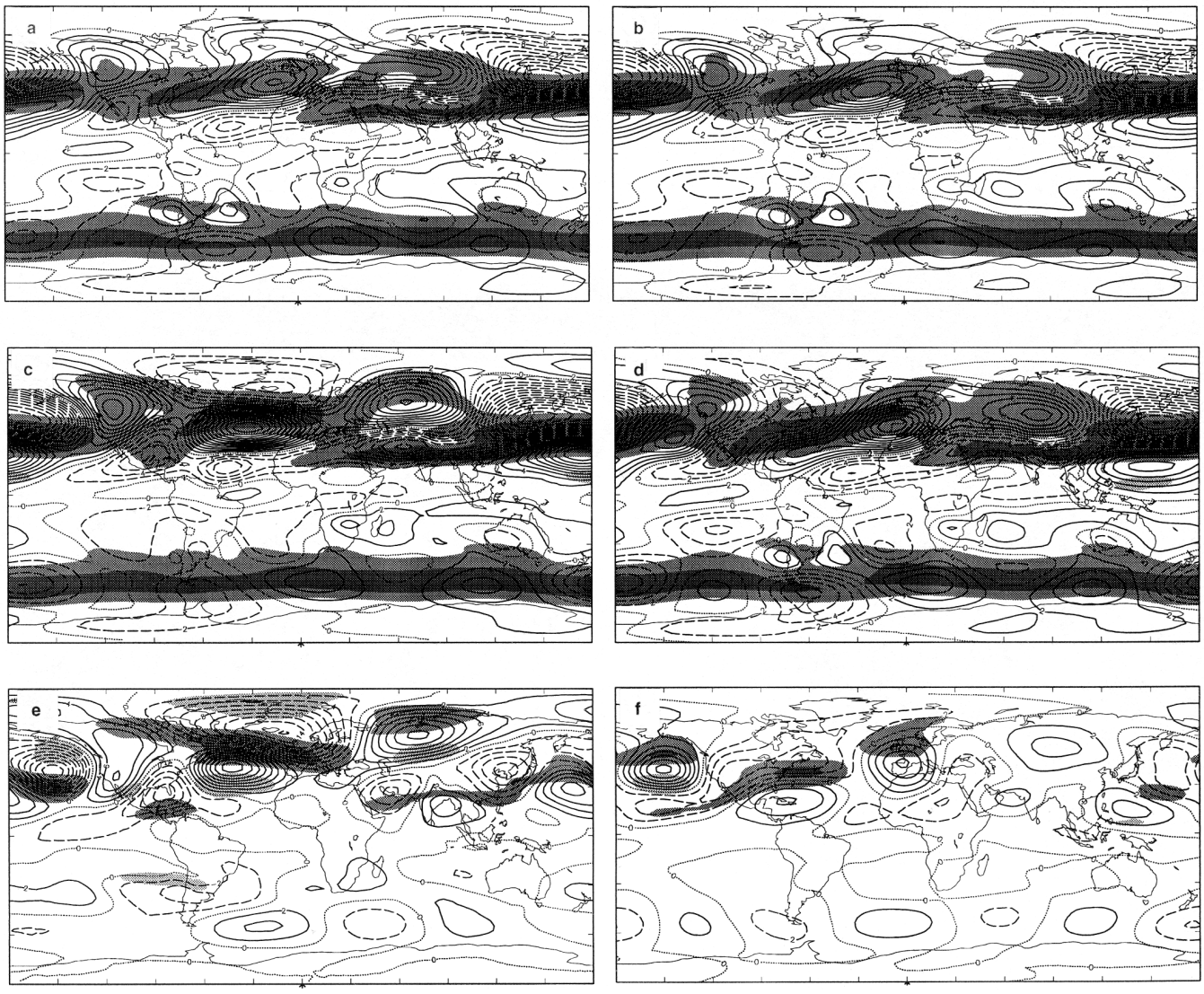

Fig. 7a–f The distribution of eddy stream function at 500 hPa and zonal wind at 500 hPa in DJF. **a** and **b** PD with prescribed and computed SSTs; **c**, **d** LGM with prescribed and computed SSTs; **e**, **f** the corresponding anomalies between LGM and PD. Contour intervals are $2.0 \times 10^6\ m\,s^{-2}$ with *negative* values *dashed*. *Light shading* indicates easterly greater than $10\ m\,s^{-1}$ in **a**, **b**, **c** and **d**, and *medium and dark shading* indicate westerly greater than $10\ m\,s^{-1}$ and $20\ m\,s^{-1}$, respectively. In the anomalies fields, the *same shading* scales correspond to easterly greater than $5\ m\,s^{-1}$ and, westerly greater than $5\ m\,s^{-1}$ and $10\ m\,s^{-1}$ respectively

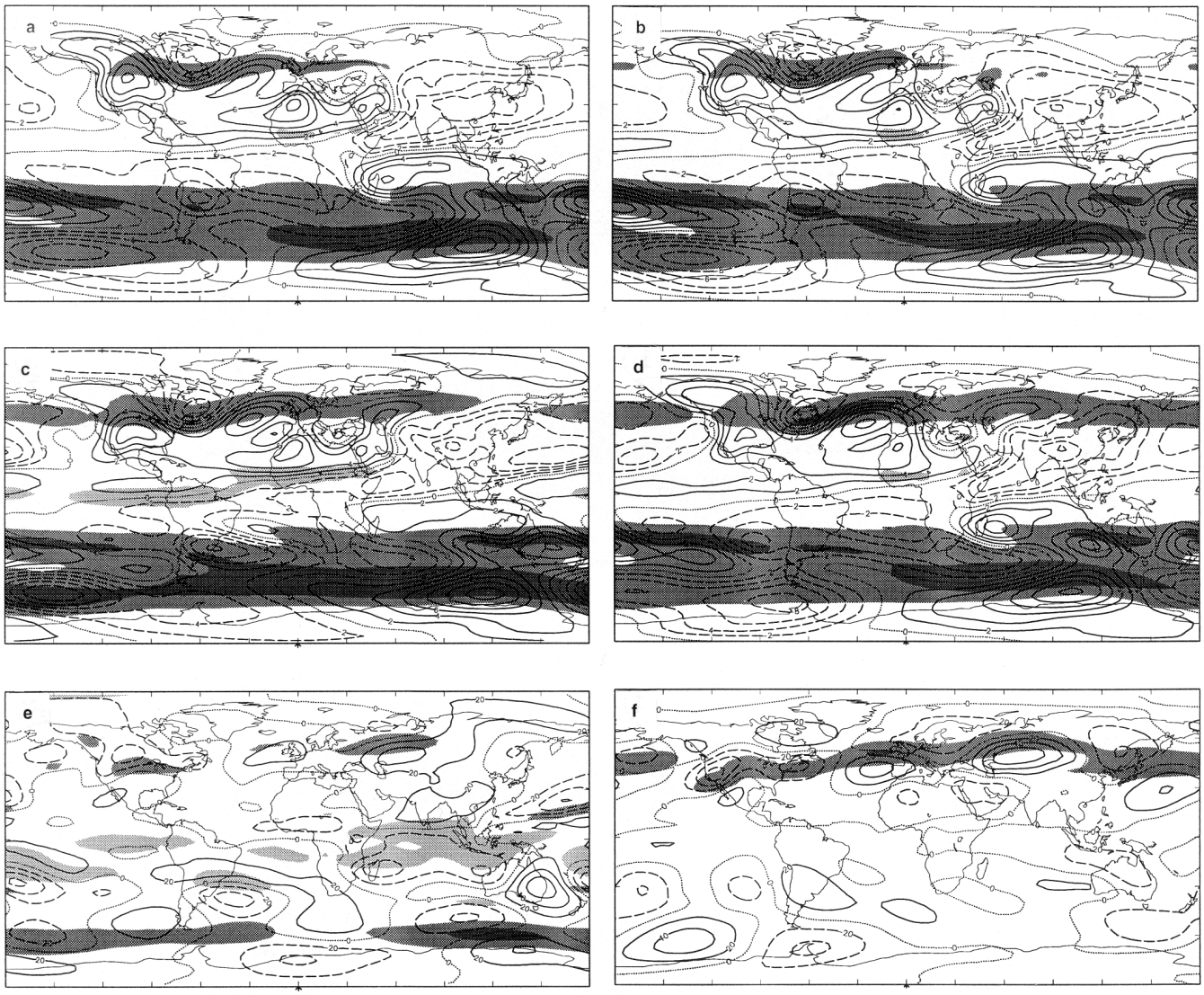

Fig. 8a–f as Fig. 7, but for JJA

ridge over northwestern America and trough in northeastern America, tilting from southwest to northeast are enhanced. i. e., the Laurentide ice sheet enhances the upstream long wave ridge and the downstream long wave trough. The north Atlantic ridge in the LGM simulations extends downstream to central Siberia with a secondary high centre there. However, the strength of the north Atlantic and central Siberian ridges in the LGM simulation with prescribed SSTs are much stronger than that in the simulation with computed SSTs. The changes in planetary wave patterns over the north Pacific in the LGM simulation with prescribed SSTs are opposite to those in the LGM simulation with computed SSTs. In the simulation with prescribed SSTs, the north Pacific trough shifts eastward slightly and intensifies while in the LGM simulation with computed SSTs it weakens. The upper level jet over the north Atlantic is significantly altered. The jet shifts downstream and northward, and its strength is enhanced in the LGM simulations. However, the splitting of the jet by the Laurentide ice sheet is not pronounced although the split flow structure over North America exists. The upper level jet over the eastern north Pacific shifts slightly equatorward in the LGM simulation with prescribed SSTs and polewards in the simulation with computed SSTs, consistent with the changes in planetary waves. The planetary waves in the Southern Hemisphere are weak and hardly change in the LGM simulations.

In JJA, the effect of ice age boundary conditions has a relatively minor effect on planetary waves in both hemispheres. The zonal wind over the north Atlantic increases in the LGM simulations, especially in the simulation with computed SSTs. This enhancement is consistent with the changes in low level baroclinicity which is enhanced over this region (Fig. 4d). In the

Southern Hemisphere, the westerlies around 60 °S are enhanced in the simulation with prescribed SSTs while it hardly changes in the simulation with computed SSTs, due to the lack of extensive sea ice in the LGM simulation with computed SSTs.

The planetary waves and upper level circulation are sensitive to the SSTs or more specifically to the sea-ice distribution. Changes in sea ice introduce changes in planetary waves and storm track activity, which in turn alters large-scale precipitation distribution and the pattern of latent heat release. Storm track activity and latent heat release are important ingredients in maintaining planetary waves (Valdes and Hoskins 1989). It is expected that changes in either of them would induce significant changes in the planetary waves.

6 Response of storm track activity

The presence of extensive ice sheets and sea ice at the LGM induces significant changes in the baroclinic structure of the atmosphere. Land-sea temperature contrasts are of primary importance for transient developing systems at the PD, whereas the temperature contrasts over the sea ice are the most important feature as regards transient eddy activity at the LGM. This is particularly true over the north Atlantic. Figures 9 and 10 give the high pass transient eddy heat flux at 700 hPa for the PD, LGM and the corresponding anomalies for the DJF and JJA, respectively. The high pass transient eddy activity shows the regions of

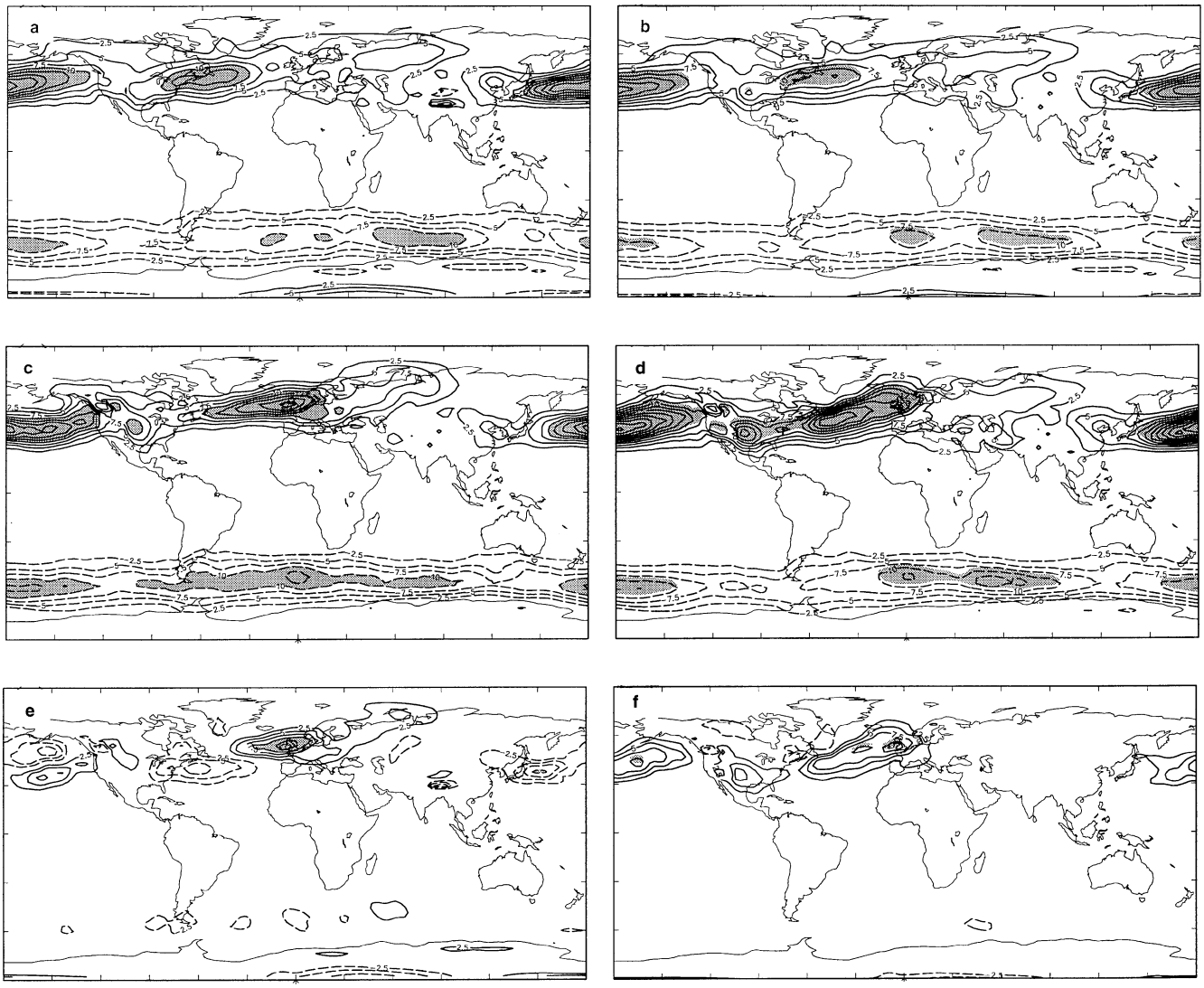

Fig. 9a–f The high pass transient eddy heat flux at 700 hPa in DJF. **a**, **b** PD with prescribed and computed SSTs; **c**, **d** LGM with prescribed and computed SSTs; **e**, **f** the corresponding anomalies between LGM and PD. Contour intervals are 2.5 K m s^{-1} with *absolute values* greater than 10 K m s^{-1} *shaded*

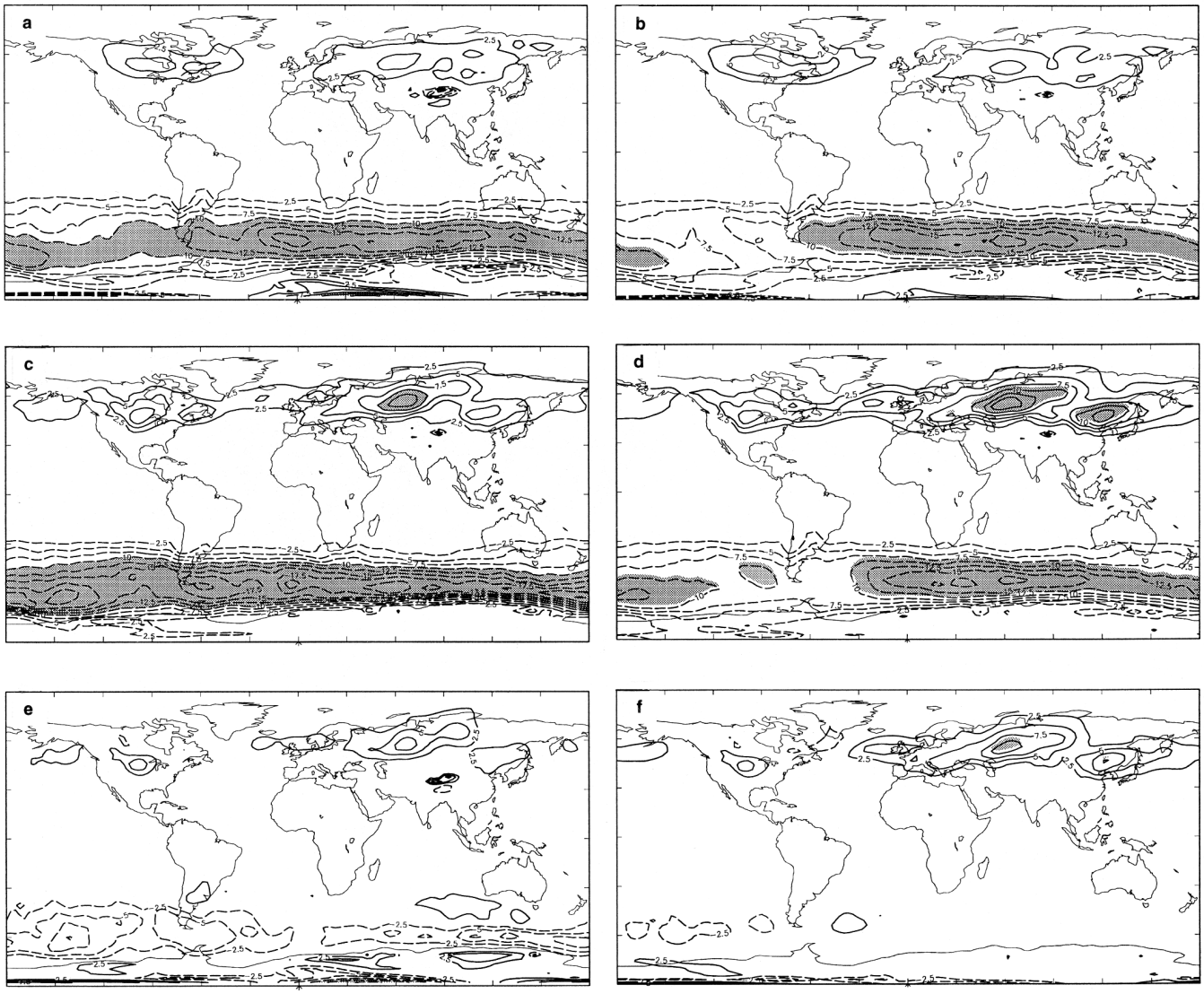

Fig. 10a–f As Fig. 9, but for JJA

maximum high-frequency variability, or "storm tracks". In DJF, the simulated positions and strengths of the three major storm tracks in the north Atlantic, north Pacific and Southern oceans are in reasonable agreement with the ECMWF analyses (Hoskins et al. 1989). The model also captures the slight northward tilt of the north Atlantic storm track. In JJA, the north Atlantic and north Pacific storm track are weak. Their positions are similar to the analysis, but the strengths are slightly underestimated. The Southern Ocean storm track is in good agreement with the analysis shown by Hoskins et al. (1989).

Significant changes occur for the two Northern Hemisphere storm tracks in the LGM simulations. In the LGM simulation with prescribed SSTs, the largest changes occur at the end of the storm track in the Pacific. The peak intensity is unaltered, but there is a downstream and equatorward shift of about 5°. This is consistent with a similar equatorward shift in the sea-ice edge, and hence in the maximum surface temperature gradient. The changes in the north Atlantic storm track are more complicated. The region of maximum eddy activity is considerably more confined meridionally, but extends much further into Europe. These changes are generally consistent with the changes in surface temperature gradient. The temperature gradients at the edge of the sea ice result in the midlatitude depressions closely following the edge of the sea ice. The sharpness of the storm track is a result of the relative efficiency with which the depressions can transport heat, and the relatively narrow meridional band over which heat needs to be transferred with such strong temperature gradient (Hall et al. 1996a).

For the PD simulation with computed SSTs, generally the characteristics of the three storm tracks are very similar to those with prescribed SSTs. However, in

the LGM simulation with computed SSTs, there are significant changes in both the north Atlantic and north Pacific storm tracks, compared with the simulation with prescribed SSTs. Both storm tracks are enhanced in the LGM simulation with computed SSTs. The enhancement of the north Pacific storm track is consistent with the extensive sea-ice cover which enhances the meridional temperature gradient along the north Pacific sea-ice edge. However, over the north Atlantic, the meridional temperature gradient in the LGM simulation with computed SSTs is not as strong as that in the simulation with prescribed SSTs, but the storm track is much enhanced. This enhancement may be due to the interaction between the north Pacific and Atlantic storm tracks. The strong baroclinic waves initiated in the north Pacific storm track propagate downstream. They may act as the initial disturbance to trigger nonmodal growth (Farrell 1984) processes over the north Atlantic baroclinic zone before they are dissipated in downward propagation. This aspect of the simulation requires further work.

The downstream development of the north Atlantic storm track steers the storms towards southern Europe and away from Greenland. This would reduce the snow accumulation over Greenland at LGM. The mass budget over various ice sheets will be discussed in Sect. 7.3.

In JJA, baroclinicity is much weaker in the Northern Hemisphere. The Northern Hemisphere transient eddy heat flux at 700 hPa, as shown in Fig. 10, is very weak over the north Atlantic in the PD simulation, and only strengthens slightly at LGM. However, the transient eddy activity along the southern edge of the land ice sheets increases, due to the enhanced temperature contrast between land and ice sheet in JJA at the LGM. In the Southern Hemisphere, the shape of the high pass transient eddy heat flux are similar in the PD simulations. Its intensity is increased in the LGM simulation with prescribed SSTs, a direct effect of the enhanced temperature gradients along the sea-ice edge based on the CLIMAP SST.

7 Resultant changes in surface hydrology

7.1 Precipitation

Considering the tremendous changes in the transient eddy activity in the Northern Hemisphere in DJF and the significant differences in the LGM simulation with computed SSTs from that with prescribed SSTs, one would expect significant changes in the associated precipitation in the region, due to condensation as warm, moist air is moved upwards and polewards. Precipitation arising from this large-scale condensation process does indeed increase, as shown in Fig. 11, which gives precipitation rate anomalies in DJF between the LGM simulations and the PD simulations due to large-scale and convective condensation process. The changes in large-scale precipitation closely follow the changes in storm track activity discussed in the previous section. The large-scale precipitation is meridionally confined and increases over the north Atlantic storm track regions. The downstream development of the north Atlantic storm track in the two LGM simulations steers the storms toward southern Europe and away from Greenland. As a result, the large-scale precipitation over Greenland decreases and it increases over Mediterranean region. There is also an increase in large-scale condensation on the northern west coast of North America in the LGM simulation with prescribed SSTs, consistent with the eastward migration of the Pacific storm track. The meridional confinement and enhancement of the large-scale precipitation over the north Pacific is also consistent with changes in storm track activity.

The changes in large-scale condensation over mid-latitudes are to some extent compensated for by changes in the precipitation due to deep convection. Over sea ice in the Northern Hemisphere, the air is dry, cold, stable at the LGM. As a result, there is a corresponding reduction in deep convection and the associated convective precipitation. Over tropical land areas, the convective precipitation decreases due to cooler climate.

The changes in large scale and convective precipitation in JJA are shown in Fig. 12. There are considerable increases in large-scale condensation over the Laurentide ice sheet and over southern part of the Fennoscandian ice sheet. These increases relative to the PD spread into the north Pacific and north Atlantic. These changes in large-scale precipitation are in agreement with the enhancement of storm track activity. There is also some degree of compensation due to the reduction in convective precipitation, particularly over the western north Atlantic, and at high latitudes in North America and Asia. The largest discrepancy over land in convective precipitation changes with prescribed SSTs and computed SSTs exists over southwest North America and South America. This discrepancy in precipitation changes is associated with circulation changes outlined in Sect. 5.1, a direct effect of changes in local circulation due to differences in SSTs.

The changes in precipitation over the oceans are more complex and are not in good agreement between the simulations with prescribed and computed SSTs. This is true for both DJF and JJA. Changes in precipitation in the simulation with prescribed SSTs follow the imposed changes in SSTs. Precipitation over warm regions increases while it decreases over cold regions. In contrast, the precipitation maximum along the ITCZ in the LGM simulation with computed SSTs shifts southward relative to the PD simulation, following the changes in the computed SST maximum. As a result, precipitation in the LGM simulation with computed SSTs decreases on the north side of equator

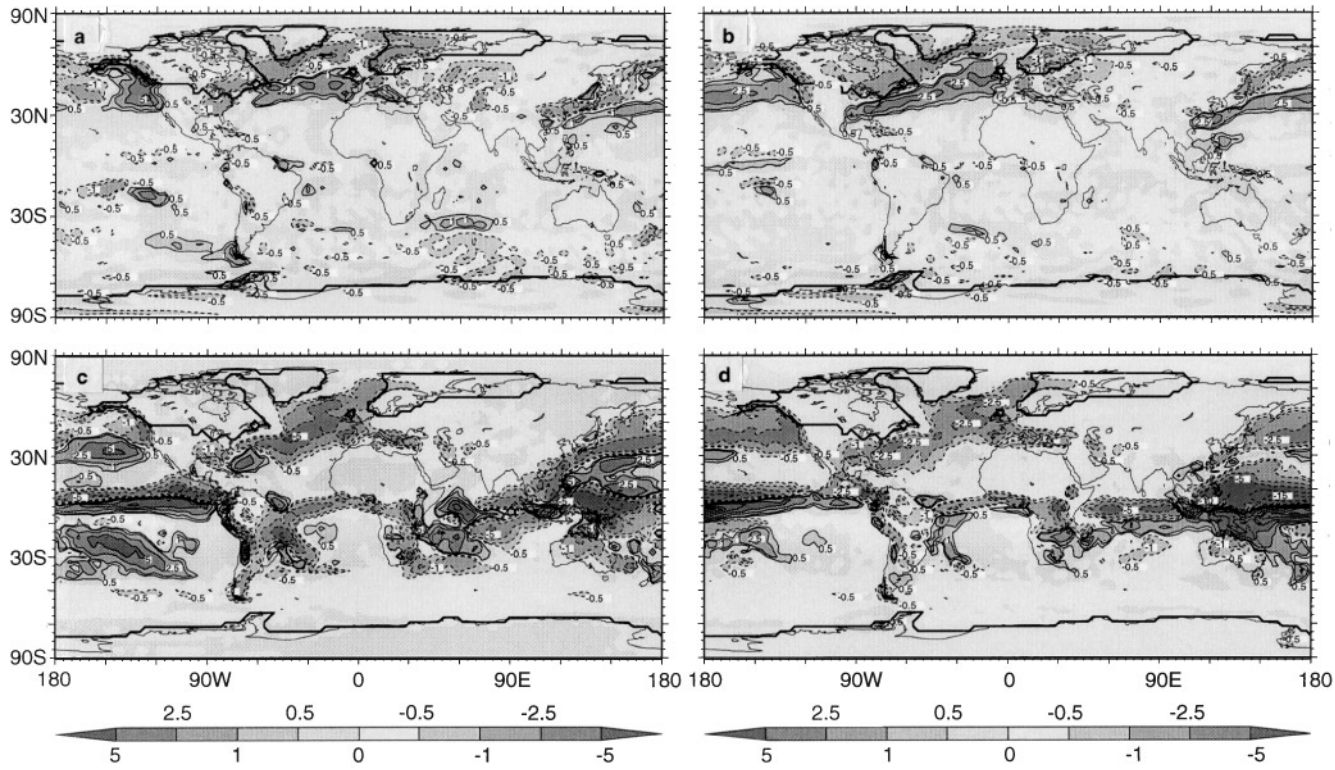

Fig. 11a–d The distribution of precipitation anomalies (mm day^{-1}) in DJF due to **a**, **b** large-scale and **c**, **d** convective condensation between the LGM and PD simulations with **a**, **c** prescribed SSTs and **b**, **d** computed SSTs. The *thick line* outlines the extent of ice sheets at LGM

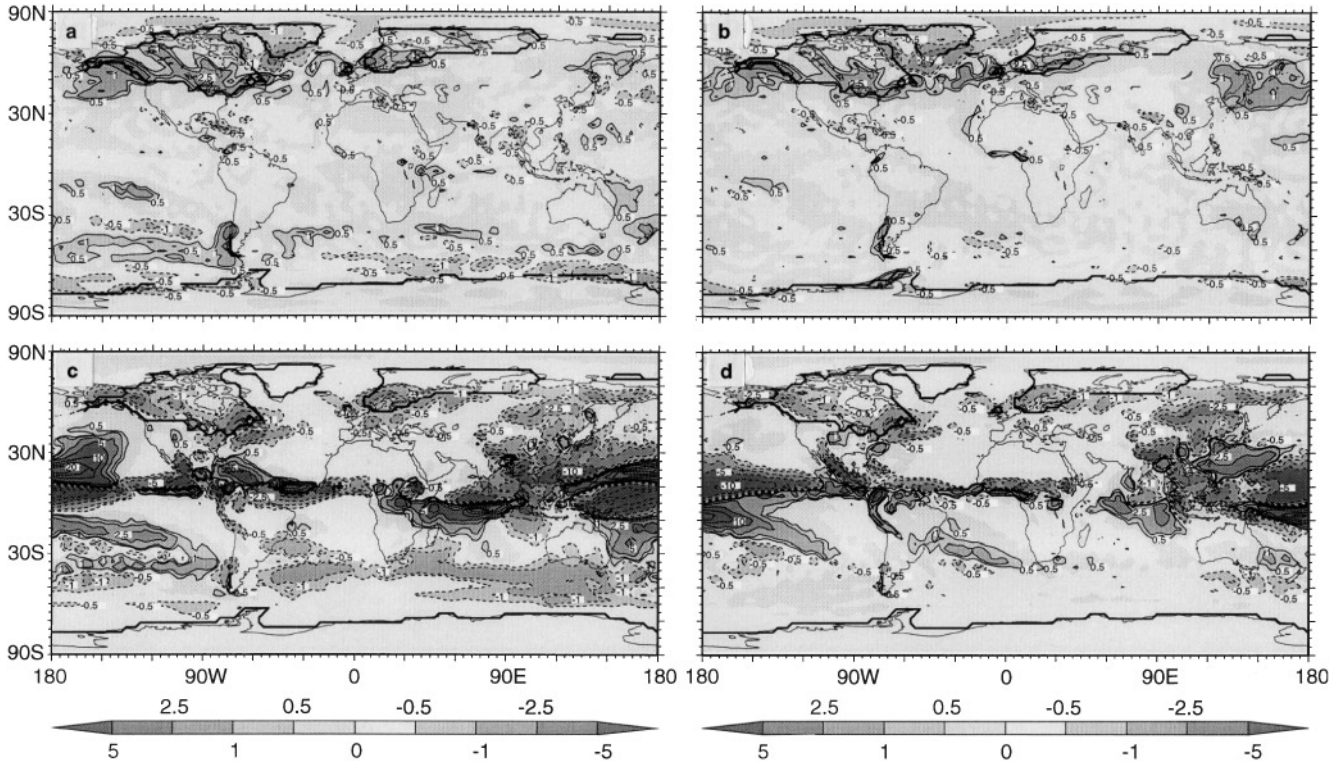

Fig. 12 As Fig. 11, but for JJA

and increases on the south side of it over tropical ocean regions in both seasons.

Figure 13 shows the changes in annual mean total precipitation. The main signal is of the drier conditions over the Eurasian continent, large parts of Africa, and Australia. Over tropical continents, the changes in annual mean precipitation follow the changes in summer convective precipitation. The opposite signal of changes in annual mean precipitation over South America and southwestern North America in the LGM simulations with prescribed and computed SSTs are a result of the convective precipitation differences in the two regions.

7.2 Soil moisture

Generally, over the continents outside the snow-covered areas and land ice sheets, soil moisture changes closely follow the changes in total precipitation (not shown). Soil moisture at mid- and high latitudes over the continents outside snow-covered areas and land ice sheets decreases in the LGM simulation. These characteristics are the same in the simulation with computed SSTs in most regions. However, the soil moisture changes over southwestern North America and South America in the simulation with computed SSTs are opposite to those in the simulation with prescribed SSTs. The differences are related to the differences in changes in convective precipitation in JJA, resulted from local circulation differences due to SSTs.

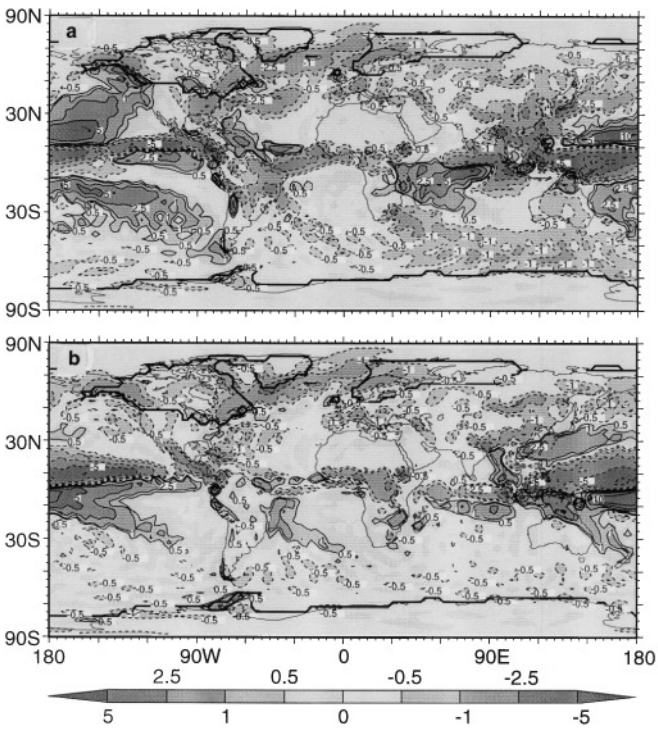

Fig. 13a, b The distribution of annual mean total precipitation anomalies (mm day^{-1}) between the LGM and PD simulations for **a** prescribed SSTs; **b** computed SSTs

7.3 Ice-sheet mass balance

Large changes in storm track activity result in changes in precipitation distribution, which in turn induces changes in mass balance over land ice sheets.

Table 3 compares their information on the snow accumulation rate and those simulated by the model for the PD and LGM. For the PD simulations, the accumulation rates over Greenland and the Antarctic are in broad agreement with observation. The notable difference between the Greenland and Antarctic ice sheets is evident. Over Greenland there is significant ablation. In contrast, over the Antarctic ablation is a negligible component in the total mass budget because the Antarctic experiences a much colder climate. The model also captures these features in the PD simulations. However, the net accumulation rate over the Greenland ice sheet in the PD simulation with computed SSTs is larger than observation and the PD simulation with prescribed SSTs. This difference is mainly due to the reduction in ablation in the PD simulation with computed SSTs because the summer surface air temperature over Greenland is about 1.5 °C colder. For the PD simulation with computed SSTs, the sea-ice extent around the Antarctic is not as extensive as that in the simulation with prescribed SSTs and also SSTs around the Antarctic are a few degrees warmer. As a result, the moisture transport to the Antarctic increases, resulting in an increase in snowfall and hence in snow accumulation.

The Greenland and Antarctic ice sheets expand slightly at the LGM due to the lowering of sea level by 105 m. In the LGM simulation, the mass budget characteristics over Greenland are quite different from the PD simulation. The ablation is negligible. The net accumulation rate over Greenland is consistent with the estimated snow accumulation rate derived from the oxygen isotopic composition of ice in the deep core by Kapsner et al. (1995). The reduction of the net snow accumulation rate is mainly due to the reduction in snowfall which is the direct result of the colder climate and downstream shift of the north Atlantic storm track. The downstream development of the north Atlantic storm track steers the storms towards southern Europe and away from Greenland. Over the Antarctic, the features of the snow mass budget in the LGM simulations are similar to those of the PD simulations because changes in the storm track activity are smaller and the air temperature in this region is very low both for the PD and LGM.

Generally, over the Laurentide and Fennoscandian ice sheets, there is net snow accumulation. This feature is true for both simulations with prescribed SSTs and

Table 3 Mass of snow cover in the model for various ice sheets. The observation is based on Warrick and Oerlemans (1990)

			Prescribed SSTs		Computed SSTs	
		Observation	PD	LGM	PD	LGM
Greenland ice sheet	Area (10^{12} m^2)	1.68	2.09	2.44	2.09	2.44
	snowfall (kg m^{-2} yr^{-1})	318.5	452.2	124.1	480.8	91.9
	Net accumulation rate (kg m^{-2} y^{-1})	151.8	166.1	119.3	256.5	83.4
	Ablation (kg m^{-2} y^{-1})	166.7	286.1	4.8	224.3	8.5
Antarctic ice sheet	Area (10^{12} m^2)	11.97	12.16	14.63	12.16	14.63
	snowfall (kg m^{-2} y^{-1})	183.8	150.9	135.1	178.2	180.8
	Net accumulation rate (kg m^{-2} y^{-1})	175.4	138.8	133.2	159.6	165.2
	Ablation (kg m^{-2} y^{-1})	8.4	12.1	1.9	18.6	15.6
Laurentide ice sheet	Area (10^{12} m^2)			15.3		15.3
	snowfall (kg m^{-2} y^{-1})			469.0		350.7
	Net accumulation rate (kg m^{-2} y^{-1})			92.1		156.0
	Ablation (kg m^{-2} y^{-1})			376.9		194.7
Fennoscandian ice sheet	Area (10^{12} m^2)			8.59		8.59
	snowfall (kg m^{-2} y^{-1})			319.0		297.2
	Net accumulation rate (kg m^{-2} y^{-1})			160.2		205.0
	Ablation (kg m^{-2} y^{-1})			158.8		92.2

with computed SSTs. The ablation over the Laurentide ice sheet represents about 2/3 of the snowfall while for the Fennoscandian ice sheets it represents about 40%. However, the difference in accumulation rate over the Laurentide ice sheet in the two LGM simulations is due to the extensive sea-ice cover in DJF and cold SSTs in JJA over north Pacific, upstream of Laurentide ice sheets in the simulation with computed SSTs.

The geographical distributions of net snow accumulation rate in the LGM simulations over the Northern Hemisphere are given in Fig. 14. Over the Laurentide ice sheet, both the LGM simulations with prescribed and computed SSTs suggest that there is net ice loss over the southern edge of the Laurentide ice sheet. In contrast, there is net ice gain over other parts of the Laurentide ice sheet. The large net accumulation rates over the southwest edge of the Cordilleran ice sheet is due to the decrease in ablation. There is also net snow accumulation over the Fennoscandian ice sheet. Generally, the net accumulation over the southern part is larger than that over the northern part.

There is also net snow accumulation over central and east Siberia, and over the Tibetan Plateau. The net accumulation over those three regions is due to the decrease in ablation rather than the increase in precipitation. These are also the regions of greatest sensitivity for ice initiation (Dong and Valdes 1995).

8 Discussion

The LGM climate represents extremely cold climate conditions. It involves large changes in surface boundary conditions, namely ice sheet extent, changes in SST, sea level and CO_2.

A variety of experiments has been performed to simulate LGM climates (e.g. Broccoli and Manabe 1987; Manabe and Broccoli 1985a,b; Kutzbach and Guetter 1986; Lautenschlager and Herlerich 1991; Rind 1987; Joussaume 1993; Hall et al. 1996b). All of these studies used the CLIMAP ice-sheet reconstruction and

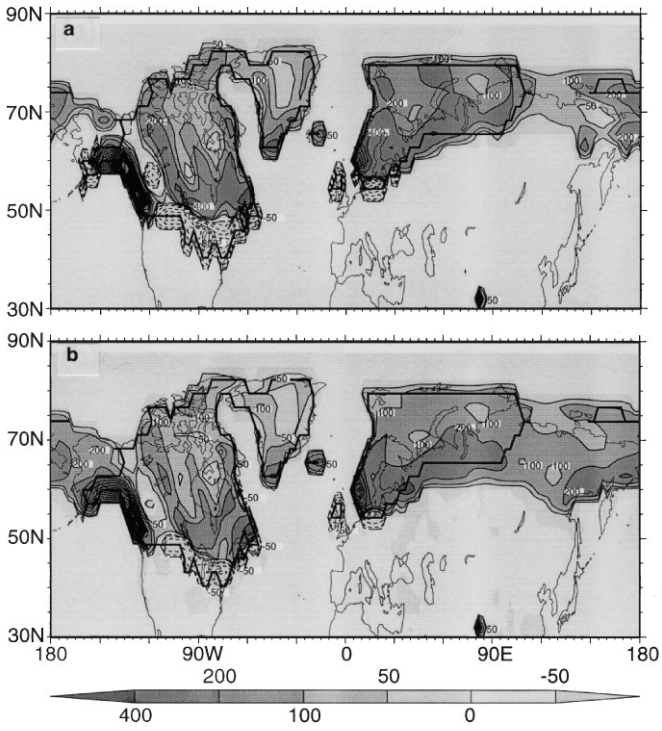

Fig. 14a,b The distribution of net snow accumulation rates (kg m^{-2} yr^{-1}) over northern mid-high latitude regions. Accumulation shown by *solid lines* and ablation by *dashed lines*. *Thick line* gives ice-sheet extent. **a** LGM with prescribed SSTs, and **b** LGM with computed SSTs

either the CLIMAP SST reconstruction or predicted SSTs using a mixed-layer ocean. However, there is uncertainty in the CLIMAP SST reconstruction. Therefore, it is natural to ask how sensitive the simulated climate changes are to the SST differences. This work addressed this question. In addition, by comparing the simulations using the new ice-sheet reconstruction with those using the CLIMAP reconstruction (Hall et al. 1996b), we can investigate the impact of the different ice sheet reconstructions on the LGM climates.

For globally averaged features, the UGAMP GCM has a quantitatively similar response to the GCMs mentioned. This feature is similar to the LMD model reported by Ramstein and Joussaume (1995). However, differences appear in local climates. The splitting of the upper tropospheric jet by the Laurentide ice sheet reported by Kutzbach and Guetter (1986), and Manabe and Broccoli (1985a) is not as pronounced in our simulations (both of these models were considerably lower resolution than that of UGAMP). Felzer et al. (1996) also found no indication of a split jet, using the NCAR CCM1. There are significant changes in planetary waves and storm track activity in LGM simulations. The storm tracks are sharper, particularly in the north Atlantic, and they line up along the sea-ice edge. These characteristics are not very sensitive to the ice-sheet reconstruction. However, they are sensitive to the distribution of SSTs, more specifically to the distribution of sea ice. The simulation using the CLIMAP ice-sheet reconstruction shows similar characteristics to the simulation with Peltier's (1994) reconstruction. A sensitivity experiment with the new ice-sheet reconstruction but with the present-day SST distribution results in the north Atlantic storm track and planetary waves over the north Atlantic sector being different from either the PD structures or LGM structures, indicating that both the sea-ice distribution and land ice sheets play a decisive role on the changes in the north Atlantic storm track activity and have an important effect on the circulation and planetary waves. This is illustrated in Fig. 15, which displays the planetary waves and dynamical storm track activity in DJF for the simulation with the CLIMAP ice sheet reconstruction (Hall et al. 1996b) and the SST sensitivity experiment (based on 3 y mean). The split of the flow over North America in the simulation with the CLIMAP ice-sheet reconstruction is more pronounced than in the simulation with the Peltier's (1994) ice-sheet reconstruction, indicating the sensitivity of flow over North America to ice-sheet reconstruction. However, the downstream jet over the North Atlantic is similar in the two simulations with different ice-sheet reconstructions. In the SST sensitivity experiment, in comparison with the PD simulation (Fig. 6a), the North Atlantic jet is enhanced due to the enhanced land-ocean temperature contrast. However, the downstream shift is not pronounced and the jet structure is more similar to the PD simulation. The sensitivity of the glacial climates to the extent of north Atlantic sea ice was also pointed out by Kutzbach and Ruddiman (1993) using the NCAR GCM. A more detailed comparison of various aspects of the simulated LGM climates by different GCMs with identical boundary conditions is currently being performed as part of the PMIP.

The mass balance over various ice sheets is one of the major factors determining the response of the ice sheet to external forcing. The quantitative accumulation rates should not be taken too literally. The GCM includes no physics related to the compaction of snow into ice, or calving of icebergs, etc., This would require a detailed ice-sheet model similar to Verbitsky and Oglesby (1992). However, the GCM results provide a potential input into the ice-sheet models, either directly through the precipitation rate or indirectly by using the moisture flux convergence. We have shown that the T42 version of the model reproduces many aspects of the mass budget characteristics over the two ice sheets.

The Laurentide and Fennoscandian ice sheets in our LGM simulations are not in mass balance in both versions. The net mass gains over the central and northern parts of both ice sheets dominate the mass loss over the southern margins. As a result, the area averaged net accumulation over the two ice sheets in

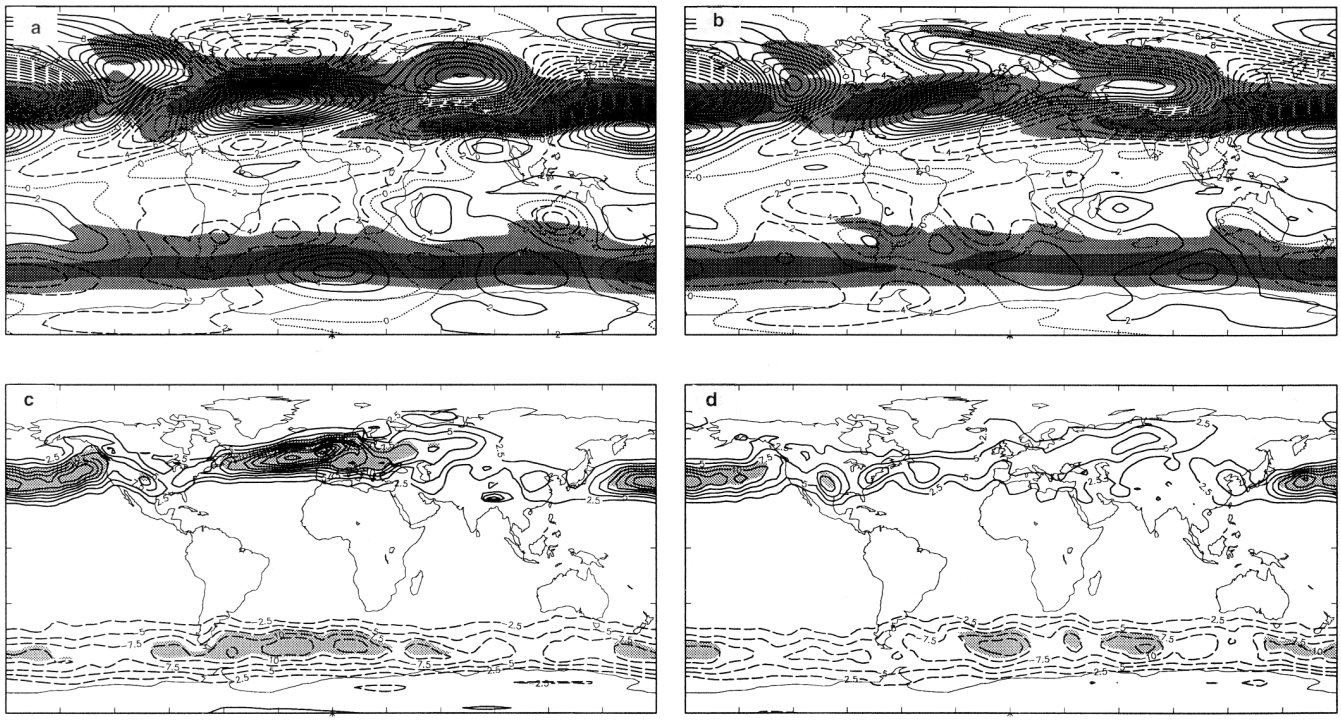

Fig. 15a–d The distribution of eddy stream function (10^6 m s^{-2}) at 500 hPa and zonal wind (m s^{-1}) at 500 hPa (**a**, **b**) and high pass transient eddy heat flux (km s^{-1}) at 700 (**c**, **d**) in DJF. **a** and **c** is the LGM simulation with the CLIMAP ice sheet and SST reconstructions; **b** and **d** is the sensitivity experiment with Peltier's (1994) ice-sheet reconstruction but with PD SSTs

the LGM simulation is positive with a resulting time scale of 1500–2000 y for an ice sheet to build upto 2000 m thick. In the LGM simulations, it has been shown that Siberia and the Tibetan Plateau are glaciation sensitive regions. This subject was discussed in detail in Dong and Valdes (1995) for the Northern Hemisphere glaciation studies.

9 Conclusions

The effect of ice age boundary conditions on climates has been investigated in the framework of PMIP using the UGAMP GCM based on two simulations. One used prescribed SSTs and the other used a 50 m mixed-layer ocean model to compute SSTs with prescribed ocean heat fluxes.

Both the continental ice sheets and sea-ice extent during the LGM are important factors responsible for changes in planetary waves and storm tracks, which in turn, affect regional climates. Our model results also indicate that the sea-ice extent over the north Atlantic plays a crucial role in changes in the Atlantic storm track while the different land ice sheet reconstructions have only a minor effect. Substantial changes in storm track activity strongly affect the supply of heat and moisture into the continental ice sheets, resulting in changes in the ice mass budget. Both the Laurentide and Fennoscandian ice sheet are fed by snowfall over the centre and northern parts and eroded by ablation over their southern edges.

Comparing the predicted land temperatures to observational evidence does not discriminate between the computed and prescribed SST simulations. Both experiments show generally good agreement between the model and data, but problems with low-latitude changes exist.

The Asian and African summer monsoon circulations weaken due to the decreased land-sea thermal contrast and much reduced summer convective activities over the monsoon regions in the LGM simulations. As a result, precipitation and soil moisture are reduced. These changes in hydrology mimic the geological evidence of drier and colder climates at the LGM.

It has been shown that the computed SSTs are generally in agreement with the CLIMAP reconstruction. However, there are significant regional differences. The sea-ice extent around the Antarctic is underestimated although there is the possibility that CLIMAP overestimated the sea-ice extent at the LGM (Burckle et al. 1982). The other major discrepancy occurs in the Pacific warm pool in low latitudes where CLIMAP estimated a warming as opposed to the cooling in the model. Broccoli and Marciniak (1996), and Hewitt and

Mitchell (1996) found a similar discrepancy using the GFDL model and the UKMO model. It has been suggested that this warmth of LGM subtropical ocean is a dynamical response of the ocean to changes in atmospheric circulation (Moore et al. 1980). Such effects are not included in the simulations with a simple mixed-layer ocean model, and must await simulations with dynamic ocean models. In addition, the interpretation of past data may also be questioned. The largest disagreement between SST anomalies computed by the model and those reconstructed by CLIMAP over tropical oceans roughly parallel the geographical variations in the precision of the transfer functions used by CLIMAP to estimate SST. Prell (1985) tested these transfer functions and calculated the standard errors for each ocean basin. They range from 1.2 °C for the Atlantic transfer function used on Atlantic data to just over 3 °C for the Pacific transfer function used on Pacific data. This suggests that the Pacific, where the model-CLIMAP disagreement is most pronounced, is also a region that the uncertainties in the estimation are large.

Future work (within framework of PMIP) will examine the extent to which these results are robust to different models, and more through model-data comparisons will be made. Moreover our results have already shown the importance of the SSTs and especially the reconstruction of sea ice and suggest that an imperative for future data collection is to improve our knowledge of these quantities.

Acknowledgements Comments from Masa Kageyama on an earlier draft are appreciated. We thank Robert J. Oglesby and an anonymous reviewer for their constructive suggestions and comments. This work was funded by the EC through the grant EC5V-CT94-057. The computer time was provided by the UGAMP, which is funded by the UK National Environment Research Council.

References

Broccoli AJ, Manabe S (1987) The influence of continental ice, atmospheric CO_2, and land-albedo on the climate of the Last Glacial Maximum. Clim Dyn 1:87–99

Broccoli AJ, Marciniak EP (1996) Comparing simulated glacial climate and paleodata: a reexamination. Paleoceangraphy 11:3–14

Burckle LH, Robinson D, Cooke D (1982) Reappraisal of sea-ice distribution in Atlantic and Pacific sectors of the southern oceans at 18000 yr BP. Nature 299:435–437

CLIMAP Project Members (1981) Seasonal reconstruction of the earth's surface at the last glacial maximum. Geol Soc Am Map Chart Ser MC-36

Dong BW, Valdes PJ (1995) Sensitivity studies of northern hemisphere glaciation using an atmospheric general circulation model. J Clim 8:2471–2496

Dong BW, Valdes PJ, Hall NMJ (1996) The changes of monsoonal climates due to Earth's orbital perturbations and ice age boundary conditions. Palaeoclim Data Modell 1:203–240

Farrell BF (1984) Modal and non-modal baroclinic waves. J Atmos Sci 41:668–673

Felzer B, Oglesby RJ, Webb T, III, Hyman DE (1996) Sensitivity of a general circulation model to changes in northern hemispheric ice sheets. J Geophys Res 101:19077–19092

Hall NMJ, Dong BW, Valdes PJ (1996a) Atmospheric equilibrium, instability and energy transport at the Last Glacial Maximum. Clim Dyn 12:497–511

Hall NMJ, Valdes PJ, Dong BW (1996b) The maintenance of the last great ice sheets: a UGAMP GCM study. J Clim 9:1004–1019

Hansen J, Lacis A, Rind D, Russell G, Stone P, Fung I, Ruedy R, Lerner J (1984) Climate sensitivity: Analysis of feedback mechanisms. In: Hansen JE, Takahashi T. (eds) Climate processes and climate sensitivity. Geophys Mono 29:130–163

Harrison EF, Minnis P, Barkstrom BR, Ramanathan V, Cess RD, Gibson GG (1990) Seasonal variation of cloud radiative forcing derived from the Earth radiation budget experiment. J Geophy Res 95:18687–18703

Hewitt CH, Mitchell JFB (1996) Paleoclimate modelling intercomparison: UKMO GCM simulations for 6 kBP and 21 kBP. Climate Research Technical Note 72, Meteorological Office, Bracknell, UK

Hoskins BJ, Hsu HH, James IN, Masutani M, Sardeshmukh PD, White GH (1989) Diagnostics of the global atmospheric circulation. WCRP Rep 27

Joussaume S (1993) Paleoclimate tracers: An investigation using an atmospheric general circulation model under ice age conditions, part 1: desert dust. J Geophys Res 98:2767–2805

Joussaume S, Taylor KE (1995) Status of the Paleoclimate Modelling Intercomparison Project (PMIP). In: Proc 1st Int AMIP Sci Conf, Monterrey, USA, WCRP-92:425–430

Kapsner WR, Alley RB, Shuman CA, Anandakrishnan A, Grootes PM, (1995) Dominant influence of atmospheric circulation on snow accumulation over the past 18000 years. Nature 373:52–54

Kutzbach JE, Guetter PJ (1986) The influence of changing orbital parameters and surface boundary conditions on climate simulations for the past 18000 years. J Atmos Sci 43:1726–1759

Kutzbach JE, Ruddiman WF (1993) Model description, external forcing, and surface boundary conditions. In: Wright HE, Jr, Kutzbach JE, Webb T. III, Ruddiman WF, Street-Perrott FA, Bartlein PJ (eds) Global climates since the Last Glacial Maximum. University of Minnesota Press, pp 12–23

Lautenschlager M. Herterich K (1990) Atmospheric response to ice-age conditions-climatology near the earth's surface. J Geophys Res 95:22547–22557

Legates DR, Willmott GG (1990) Mean seasonal and spacial variability in gauge corrected, global precipitation. Int J Climatol 10:111–127

Manabe S, Broccoli AJ (1985a) The influence of continental ice sheets on the climate of an ice age. J Geophys Res 90:2167–2190

Manabe S, Broccoli AJ (1985b) A comparison of climate model sensitivity with data from the Last Glacial Maximum. J Atmos Sci 23:2643–2651

Moore TC, Burckle L, Geitzenauer K, Luz B, Molina-Cruz A, Robertson J, Sachs H, Sancetta C, Thiede J, Thompson P, Wenkam C (1980) The reconstruction of sea surface temperatures in the Pacific ocean of 18000 BP Mar Micropaleontol 5:215–247

Peltier WR (1994) Ice age paleotopography. Science 265:195

Prell WL (1985) The stability of low latitude sea surface temperatures: an evaluation of the CLIMAP reconstruction with emphasis on the positive SST anomalies. DOE Rep TRO25, US Department of Energy, Washington, D.C.

Ramstein G, Joussaume S (1995) Sensitivity experiments to sea surface temperatures, sea-ice extent and ice-sheet reconstruction, for the Last Glacial Maximum. Ann Glaciol 21:343–347

Raval A, Ramanathan V (1989) Observational determination of the greenhouse effect. Nature 342:758–761

Rind D (1987) Components of the ice age circulation. J Geophys Res 92:4241–4281

Rind D, Peteet D (1985) Terrestrial conditions at the last glacial maximum and CLIMAP sea surface temperature estimates: are they consistent? Quat Res 24:1–22

Slingo JM, Blackburn M, Betts A, Hodges K, Hoskins BJ, Miller M, Steenman-Clark, Thuburn J (1994) Mean climate and transience in the tropics of UGAMP GCM: sensitivity to convective parametrizations. Q J R Meteorol Soc 120: 881–922

Valdes PJ, Hoskins BJ (1989) Linear stationary wave simulations of the time-mean climatological flows. J Atmos Sci 46: 2509–2527

Velichko AA, Isayeva LL, Oreshkin DB, Faustova MA (1989) The last glaciation of Eurasia. In: Herman Y (ed) The Arctic seas: climatology, oceanography, geology, and biology. Van Nostrand Reinhold, New York, pp 729–758

Verbitsky MY, Oglesby RJ (1992) The effect of atmospheric carbon dioxide concentration on the continental glaciation of the northern hemisphere. J Geophys Res 97: 5895–5909

Warrick RA, Oerlemans J (1990) Sea level rise. In: Scientific Assessment of Climate Change. IPCC Working Group I Rep. pp 261–286

Webb RS, Rind DH, Lehman SJ, Healy RJ, Sigman D (1997) Influence of ocean heat transport on the climate of the Last Glacial Maximum. Nature 385: 695–699